J. Fluid Mech. (2013), *vol.* 726, *pp.* 226–260.
doi:10.1017/jfm.2013.213

Dispersion and nonlinearity of multi-layer non-hydrostatic free-surface flow

Yefei Bai† and Kwok Fai Cheung

Department of Ocean and Resources Engineering, University of Hawaii, Honolulu, HI 96822, USA

(Received 20 September 2012; revised 16 February 2013; accepted 18 April 2013;
first published online 31 May 2013)

Non-hydrostatic multi-layer models have become a popular tool in describing wave transformation from deep water to the surf zone, but the numerical approach lacks a theoretical framework to guide implementation and assist interpretation of the results. In this paper, we formulate a non-hydrostatic model in an analytical form for the derivation and examination of dispersive and nonlinear properties. Depth integration of the dimensionless continuity and Euler equations over each layer yields the conventional multi-layer formulation. A variable transformation converts the conventional form into an integrated series form, which provides separate descriptions of flux- and dispersion-dominated processes. Substitution of the non-hydrostatic pressure and vertical velocity in the governing equations by high-order derivatives of the horizontal velocity and surface elevation provides a direct comparison with the Boussinesq equations published in the literature. Implementation of a perturbation expansion extracts the first- and second-order governing equations with respect to the nonlinear parameter. Based on that, we derive analytical solutions of the linear dispersion and the second-order super- and sub-harmonics for up to three layers and optimize the solutions in terms of the layer arrangement. In relation to the Boussinesq equations at comparable orders of expansion, the two- and three-layer models provide slightly higher errors in shallow and intermediate water in terms of dispersion and super-harmonics, but show superior performance in describing sub-harmonics in deep water.

Key words: surface gravity waves, waves/free-surface flows

1. Introduction

Propagation of ocean waves from deep water to the shore involves a sequence of physical processes with varying spatial and temporal scales that require a slew of mathematical and numerical treatments. In addition to wave refraction and diffraction induced by bathymetric features, intrinsic properties such as dispersion, nonlinearity and breaking play an important role in coastal wave processes. Dispersion, which describes waves with different periods travelling at different speeds, determines wave transformation from deep to intermediate water. Nonlinear interactions steepen the wave profile during the shoaling process and induce long-period waves in the surf zone. Breaking and broken waves in shallow water and sheet flows on the beach are flux-dominated, involving shock-related hydraulic processes. Recent phase-resolving models based on Boussinesq and non-hydrostatic formulations, which utilize various

† Email address for correspondence: yefei@hawaii.edu

analytical and numerical approaches to address these wave processes, provide results with reasonable accuracy for practical application.

The Boussinesq equations have provided a theoretical framework to describe coastal wave transformation since their introduction by Peregrine (1967). The depth-integrated governing equations describe the vertical flow structure in terms of high-order derivatives of the horizontal particle velocity and surface elevation. Madsen, Murray & Sørensen (1991) reformulated the linear dispersion to match a [2, 2] Padé expansion in terms of the dimensionless water depth. Nwogu (1993) obtained the same order of approximation through a consistent derivation from the Euler equations with the velocity evaluated at an optimal level. Wei, Kirby & Grilli (1995) extended Nwogu's approach to include full nonlinearity of the free-surface boundary condition while maintaining the same order of dispersion approximation. Gobbi, Kirby & Wei (2000) subsequently extended the dispersion properties to a [4, 4] Padé approximation through a weighted average of the velocity potential. Madsen, Bingham & Schäffer (2003) and Madsen, Fuhrman & Wang (2006) extended the fully nonlinear Boussinesq formulations of Agnon, Madsen & Schäffer (1999) to include higher-order dispersion over mildly and rapidly varying bathymetry with an infinite power series expansion of the velocity profile. The high-order dispersion terms in the Boussinesq approach, however, produce a local anomaly prior to wave breaking that might lead to numerical instability. The eddy viscosity concept of Zelt (1991) or the roller concept of Schäffer, Madsen & Deigaard (1993) is typically implemented to account for energy dissipation due to wave breaking. Recent Boussinesq models, which utilize shock-capturing schemes with the dispersion terms deactivated locally, describe breaking waves as bores without the use of empirical dissipation mechanisms (Kazolea *et al.* 2012; Roeber & Cheung 2012; Shi *et al.* 2012; Tonelli & Petti 2012).

The non-hydrostatic approach provides an alternative to the Boussinesq equations by directly resolving the vertical flow structure to account for dispersion. This approach decomposes the pressure into hydrostatic and non-hydrostatic components in the Navier–Stokes equations (Casulli 1995). The continuity equation for an incompressible fluid provides a Poisson equation for the solution of the non-hydrostatic pressure. Casulli & Stelling (1998) and Stansby & Zhou (1998) demonstrated the important role of the non-hydrostatic pressure and vertical flow structure over a varying bottom even in shallow water. The dispersion properties can be improved by adding more layers without increasing the order of the spatial derivatives in the governing equations (Casulli 1999; Zhou & Stansby 1999). Stelling & Zijlema (2003) proposed a boundary-fitted coordinate system and Yuan & Wu (2004) utilized a σ coordinate to better resolve the non-hydrostatic pressure near boundaries. Zijlema & Stelling (2005) proposed a multi-layer non-hydrostatic model, which reproduces linear dispersion properties in deep water with just two fluid layers. Instead of full implementation of a boundary-fitted coordinate system, Ai, Jin & Lv (2011) arranged the vertical velocity at cell centre and developed a three-dimensional model with a finite-volume scheme for free-surface flows. Ai & Jin (2012) demonstrated that the model requires up to ten layers to accurately describe the vertical distributions of the velocity and the non-hydrostatic pressure. Ma, Shi & Kirby (2012) expressed the Navier–Stokes equations in conservative form with a σ coordinate and developed a shock-capturing scheme to describe coastal wave transformation with three to five vertical layers.

The multi-layer formulation with first-order spatial derivatives is more amenable to practical applications. Zijlema & Stelling (2008) applied the depth-integrated formulation of Zijlema & Stelling (2005) with a wet–dry algorithm to model inundation and the momentum-conserving scheme of Stelling & Duinmeijer (2003)

to simulate wave breaking as bores and a hydraulic jump in a one-layer model. They subsequently released the multi-layer model known as SWASH (simulating waves till shore) for coastal engineering applications (Zijlema, Stelling & Smit 2011). Yamazaki, Kowalik & Cheung (2009) applied an upwind-flux approximation scheme in a one-layer model to describe energetic wave breaking, bore propagation and runup. Most importantly, the first-order spatial derivatives in the governing equations allow implementation of two-way nested grids to model wave transformation and inundation processes over a range of spatial and temporal scales (Yamazaki, Cheung & Kowalik 2011*a*). The resulting model, known as NEOWAVE (non-hydrostatic evolution of ocean wave), has been implemented in studies of the 2009 Samoa (Roeber, Yamazaki & Cheung 2010), 2009 Mentawai (Lay *et al.* 2011), 2010 Chile (Yamazaki & Cheung 2011) and 2011 Tohoku (Yamazaki *et al.* 2011*b*) tsunamis. In an effort to extend NEOWAVE's capabilities to model coastal processes, Bai & Cheung (2012) derived an alternative non-hydrostatic formulation that includes a flux-dominated and a dispersion-dominated system for a two-layer system. The resulting model provides a robust and accurate solution that captures breaking waves as bores as well as runup and drawdown on a beach. Bai & Cheung (2013) subsequently proposed a hybrid system with a parametrized non-hydrostatic pressure distribution that performs comparably with a two-layer model but at the computational expense of a one-layer model.

Despite the growing popularity of non-hydrostatic models, their dispersive and nonlinear properties have not been explored to the same extent as in studies of the Boussinesq approach (Nwogu 1993; Wei & Kirby 1995; Gobbi *et al.* 2000; Madsen *et al.* 2003, 2006). These properties modify shock formation and propagation, which in turn affect the model capabilities in handling breaking and broken waves and the subsequent runup processes (Bai & Cheung 2013). It has been a common practice to determine the number of layers sufficient for a specific application through numerical experiments. A systematic analysis of dispersion and nonlinearity is necessary to understand the merits and limitations of the non-hydrostatic approach and to guide development of the numerical frameworks. This paper extends the non-hydrostatic formulation of Bai & Cheung (2012) from a two-layer to a multi-layer system in dimensionless form that allows identification of linear and nonlinear properties. The resulting governing equations, which comprise a flux-dominated system and a dispersion-dominated system, provide a straightforward approach to derive analytical solutions of wave properties for comparison with those from the Boussinesq approach. For demonstration, we present analytical solutions of the dispersion relation and the second-order super- and sub-harmonics for the one-, two- and three-layer models, examine the layer arrangement and pressure distribution for optimization, and highlight the convergence characteristics with the number of layers. The results are evaluated with reference to the formulations and solutions from Peregrine (1967), Nwogu (1993), Wei & Kirby (1995) and Gobbi *et al.* (2000), which have comparable levels of approximation. Comparison of the solution with Stokes second-order wave theory provides an assessment of the multi-layer approach in terms of dispersion and nonlinearity.

2. Governing equations

The continuity and Euler equations provide a framework to describe fluid motions with a free surface. Implementation of characteristic length scales relevant to coastal wave transformation allows reformulation of the continuity and Euler equations in dimensionless form with the dispersion and nonlinear terms clearly identified. This

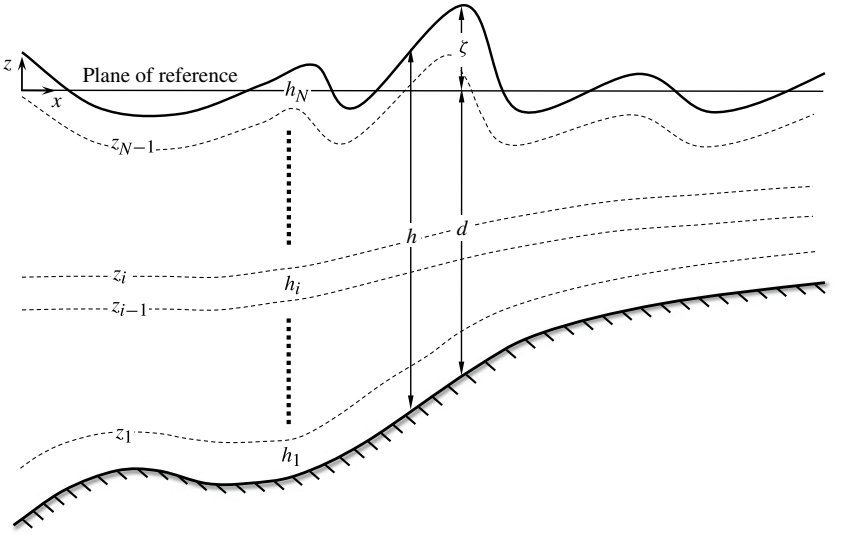

FIGURE 1. Definition sketch of a multi-layer free-surface flow.

leads to derivation of the dimensionless governing equations for the conventional multi-layer formulation that can be recast into an integrated form with separate systems for flux- and dispersion-dominated processes. The integrated form of the governing equations enables their transformation to an equivalent Boussinesq form with dispersion and nonlinear terms arranged in a hierarchy order. This allows implementation of a perturbation expansion to extract linear and nonlinear governing equations for direct comparison with the Boussinesq equations.

2.1. *Continuity and Euler equations*

Consider a two-dimensional free-surface flow over a varying bottom as in figure 1. In the Cartesian coordinate system (x, z), the variables d and ζ denote the water depth and surface elevation and $h = \zeta + d$ is the flow depth. The characteristic length scales a_0, d_0 and l_0 of the wave amplitude, water depth and wavelength give rise to the dimensionless parameters $\epsilon = a_0/d_0$ and $\mu = d_0/l_0$, which denote nonlinearity and dispersion in the governing equations. The following physical variables (primed) are then converted to dimensionless quantities as

$$x = \frac{x'}{l_0}, \quad z = \frac{z'}{d_0}, \quad t = \frac{t'}{l_0/\sqrt{gd_0}}, \quad \zeta = \frac{\zeta'}{a_0}, \tag{2.1}$$

where $\sqrt{gd_0}$ corresponds to the shallow-water celerity. The velocity (u, w) is scaled differently in the literature to achieve appropriate governing equations for specific physical problems. For non-hydrostatic free-surface flows in coastal engineering applications, the two components are typically expressed in the following dimensionless form:

$$u = \frac{u'}{\epsilon\sqrt{gd_0}}, \quad w = \frac{w'}{\epsilon\mu\sqrt{gd_0}}. \tag{2.2}$$

The nonlinear parameter ϵ scales the resulting governing equations for applications with gravity waves, while the dispersion parameter μ allows resolution of the vertical

structure even in flux-dominated flows. These parameters are instrumental should truncation of high-order terms in the governing equations become necessary.

The non-hydrostatic formulation of free-surface flows includes the pressure derived explicitly from the Euler equations. Following Casulli (1995), the dimensional pressure is decomposed into hydrostatic and non-hydrostatic components as

$$p' = g(\zeta' - z') + q', \tag{2.3}$$

where q' denotes the non-hydrostatic pressure. The scaling of the non-hydrostatic pressure will affect the form of the governing equations. A parameter n is introduced to scale the non-hydrostatic pressure with respect to the hydrostatic pressure P as

$$q = \frac{q'}{nP}. \tag{2.4}$$

When Mahadevan, Oliger & Street (1996*a*,*b*) examined the well-posedness of the non-hydrostatic approach for large-scale circulation, they balanced the vertical Coriolis acceleration with the non-hydrostatic pressure gradient by setting $n = \mu$. Marshall *et al.* (1997) discussed the use of this parameter in scaling of the governing equations for hydrostatic, quasi-hydrostatic and non-hydrostatic problems, and outlined a strategy for ocean models to perform efficiently and accurately in different spatial scales. In the hydrostatic and geostrophic limit, they found that $n = \mu^2/R_i$, where R_i is the Richardson number. Since we focus on wave dispersion and nonlinearity factors such as Coriolis effects, surface shear stress and viscous dissipation are not considered here. Vertical acceleration in the momentum equation will be fully balanced by the non-hydrostatic pressure gradient, which leads to $n = \mu^2$ in this study.

Substitution of the pressure decomposition (2.3) and the variable definitions (2.1), (2.2) and (2.4) into the continuity and Euler equations gives the dimensionless governing equations for non-hydrostatic free-surface flows as

$$\frac{\partial u}{\partial x} + \frac{\partial w}{\partial z} = 0, \tag{2.5}$$

$$\frac{\partial u}{\partial t} + \epsilon\frac{\partial u^2}{\partial x} + \epsilon\frac{\partial uw}{\partial z} + \frac{\partial \zeta}{\partial x} + \mu^2\frac{\partial q}{\partial x} = 0, \tag{2.6}$$

$$\frac{\partial w}{\partial t} + \epsilon\frac{\partial uw}{\partial x} + \epsilon\frac{\partial w^2}{\partial z} + \frac{\partial q}{\partial z} = 0. \tag{2.7}$$

The kinematic boundary conditions at the free surface and seabed become

$$w_\zeta = \frac{\partial \zeta}{\partial t} + \epsilon u_\zeta \frac{\partial \zeta}{\partial x}, \quad z = \epsilon\zeta, \tag{2.8}$$

$$w_d = -u_d\frac{\partial d}{\partial x}, \quad z = -d, \tag{2.9}$$

where u_ζ and u_d denote the horizontal velocity evaluated at the surface and bottom, respectively. The parameters ϵ and μ^2 become instrumental in identifying the nonlinear and dispersion terms in the governing equations and boundary conditions. Since $\partial u/\partial x$ and $\partial w/\partial z$ have the same order of magnitude, the dispersion parameter μ does not exist in the continuity equation (2.5). In the x direction, the horizontal derivative of the surface elevation has the same order of magnitude as the local acceleration, while the non-hydrostatic pressure gradient has an order of magnitude μ^2. In the z direction, the magnitude of the local vertical acceleration and the non-hydrostatic pressure gradient are of the same order.

2.2. *Conventional multi-layer formulation*

Accurate description of wave propagation over a varying bottom relies on the resolution of the vertical flow structure through a number of layers in a non-hydrostatic model. Zijlema & Stelling (2005) derived a depth-integrated form of the continuity and Euler equations in a multi-layer system and formulated the resulting governing equations in a conservative form. In this section, we rederive the governing equations for multi-layer flows in dimensionless form to provide a systematic account of nonlinearity and dispersion.

The water column is divided into N layers by $(N-1)$ non-crossing interfaces at z_i between the bottom and the surface, as shown in figure 1. The thickness of each layer is denoted by h_i, with $i = 1, \ldots, N$ from the bottom to the surface. As the interfaces move with the free surface over time, the layer ratio defined by

$$r_i = h_i/h \tag{2.10}$$

remains the same. This provides the location of each interface at

$$z_i = \sum_{j=1}^{i} r_j h - d. \tag{2.11}$$

Depth integration of the continuity equation (2.5) in each layer and application of Leibniz's rule yield

$$\frac{\partial}{\partial x}\int_{z_{i-1}}^{z_i} u\,\mathrm{d}z - u_{z_i}\frac{\partial z_i}{\partial x} + u_{z_{i-1}}\frac{\partial z_{i-1}}{\partial x} + w_{z_i} - w_{z_{i-1}} = 0, \tag{2.12}$$

where the subscripts z_i and z_{i-1} denote the interfaces at which the velocity is evaluated. The horizontal component $u_{z_i} = (u_i + u_{i+1})/2$ is the average from the adjacent layers, but the vertical component w_{z_i} should be distinguished from that of the interface based on a kinematic boundary condition. A relative vertical velocity Δw_{z_i} defines the difference between w_{z_i} and the vertical velocity of the interface as

$$\Delta w_{z_i} = w_{z_i} - \frac{1}{\epsilon}\frac{\partial z_i}{\partial t} - u_{z_i}\frac{\partial z_i}{\partial x}. \tag{2.13}$$

This variable facilitates transfer of mass and momentum across the interface that might become important for discontinuous flows. Depth integration of the horizontal and vertical momentum equations (2.6) and (2.7) yields

$$\begin{aligned}&\frac{\partial}{\partial t}\int_{z_{i-1}}^{z_i} u\,\mathrm{d}z + \epsilon\frac{\partial}{\partial x}\int_{z_{i-1}}^{z_i} u^2\,\mathrm{d}z + (z_i - z_{i-1})\frac{\partial \zeta}{\partial x}\\ &\quad + \mu^2\left[\frac{\partial}{\partial x}\int_{z_{i-1}}^{z_i} q\,\mathrm{d}z - \left(q_{z_i}\frac{\partial z_i}{\partial x} - q_{z_{i-1}}\frac{\partial z_{i-1}}{\partial x}\right)\right] + \epsilon u_{z_i}\Delta w_{z_i} - \epsilon u_{z_{i-1}}\Delta w_{z_{i-1}} = 0,\end{aligned} \tag{2.14}$$

$$\frac{\partial}{\partial t}\int_{z_{i-1}}^{z_i} w\,\mathrm{d}z + \epsilon\frac{\partial}{\partial x}\int_{z_{i-1}}^{z_i} uw\,\mathrm{d}z + q_{z_i} - q_{z_{i-1}} + \epsilon w_{z_i}\Delta w_{z_i} - \epsilon w_{z_{i-1}}\Delta w_{z_{i-1}} = 0. \tag{2.15}$$

The interfacial advection terms $u_{z_i}\Delta w_{z_i}$ and $w_{z_i}\Delta w_{z_i}$ also contribute to the nonlinear properties in the momentum equations and play an important role in momentum exchange when strong nonlinear advection occurs over the water column (Bai 2012).

The continuity equation (2.12) and the momentum equations (2.14) and (2.15) are formulated in terms of definite integrals that can be evaluated from assumed linear distributions of the velocity and pressure over each layer. Integration of the horizontal

and vertical velocity components is approximated as

$$\int_{z_{i-1}}^{z_i} u\,\mathrm{d}z = h_i u_i \quad \text{and} \quad \int_{z_{i-1}}^{z_i} w\,\mathrm{d}z = h_i w_i, \tag{2.16}$$

where u_i and w_i denote the average values in layer i. The integral of the quadratic velocity terms in (2.14) can be expressed as

$$\int_{z_{i-1}}^{z_i} u^2\,\mathrm{d}z = \int_{z_{i-1}}^{z_i} (u_i + \tilde{u}_i)^2\,\mathrm{d}z = h_i u_i^2 + \int_{z_{i-1}}^{z_i} \tilde{u}_i^2\,\mathrm{d}z, \tag{2.17}$$

where $\tilde{u}_i$ denotes a linear variation about the layer-averaged value. The integral of $\tilde{u}_i^2$ is commonly treated as diffusion and thus is ignored here. The same treatment also applies to the integral of uw in (2.15),

$$\int_{z_{i-1}}^{z_i} uw\,\mathrm{d}z = \int_{z_{i-1}}^{z_i} (u_i + \tilde{u}_i)(w_i + \tilde{w}_i)\,\mathrm{d}z = h_i u_i w_i + \int_{z_{i-1}}^{z_i} \tilde{u}_i \tilde{w}_i\,\mathrm{d}z, \tag{2.18}$$

in which the integral of $\tilde{u}_i \tilde{w}_i$ is ignored. Application of the trapezoidal rule gives the integrals of the non-hydrostatic pressure and vertical velocity in each layer as

$$\int_{z_{i-1}}^{z_i} q\,\mathrm{d}z = \frac{h_i}{2}(q_{z_{i-1}} + q_{z_i}), \tag{2.19}$$

$$\int_{z_{i-1}}^{z_i} w\,\mathrm{d}z = \frac{h_i}{2}(w_{z_{i-1}} + w_{z_i}). \tag{2.20}$$

The kinematic boundary conditions define the vertical velocity at the free surface and the bottom as

$$w_\zeta = \frac{\partial \zeta}{\partial t} + \epsilon u_N \frac{\partial \zeta}{\partial x}, \quad z = \epsilon\zeta, \tag{2.21}$$

$$w_d = -u_1 \frac{\partial d}{\partial x}, \quad z = -d, \tag{2.22}$$

while the dynamic boundary condition defines the non-hydrostatic pressure $q_\zeta = 0$ at the free surface.

The depth integration approximates the vertical flow structure by a piecewise linear distribution and the kinematic boundary conditions at the free surface and bottom by the layer-averaged velocity. With the integrals evaluated, the continuity and the horizontal and vertical momentum equations of layer i are given respectively as

$$\frac{\partial h_i u_i}{\partial x} - u_{z_i}\frac{\partial z_i}{\partial x} + u_{z_{i-1}}\frac{\partial z_{i-1}}{\partial x} + w_{z_i} - w_{z_{i-1}} = 0, \tag{2.23}$$

$$\begin{aligned}\frac{\partial u_i}{\partial t} &+ \frac{\epsilon}{h_i}\left(\frac{\partial h_i u_i^2}{\partial x} - u_i\frac{\partial h_i}{\partial t}\right) + \frac{\partial \zeta}{\partial x} + \frac{\epsilon}{h_i}u_{z_i}\Delta w_{z_i} - \frac{\epsilon}{h_i}u_{z_{i-1}}\Delta w_{z_{i-1}} \\ &+ \frac{\mu^2}{h_i}\left[\frac{1}{2}\frac{\partial h_i(q_{z_i} + q_{z_{i-1}})}{\partial x} - \left(q_{z_i}\frac{\partial z_i}{\partial x} - q_{z_{i-1}}\frac{\partial z_{i-1}}{\partial x}\right)\right] = 0,\end{aligned} \tag{2.24}$$

$$\frac{\partial w_i}{\partial t} + \frac{\epsilon}{h_i}\left(\frac{\partial h_i u_i w_i}{\partial x} - w_i\frac{\partial h_i}{\partial t}\right) + \frac{q_{z_i}}{h_i} - \frac{q_{z_{i-1}}}{h_i} + \frac{\epsilon w_{z_i}\Delta w_{z_i}}{h_i} - \frac{\epsilon w_{z_{i-1}}\Delta w_{z_{i-1}}}{h_i} = 0. \tag{2.25}$$

This gives rise to $3N$ governing equations for an N-layer flow system. The flows between adjacent layers are directly coupled through the relative vertical velocity (2.13) defined at the interface. Since the governing equations for each layer share the

same structure, it is straightforward to implement the formulation for any finite number of layers for development of a numerical solution.

2.3. *Integrated multi-layer formulation*

The conventional multi-layer formulation provides a direct description of the flows in the layers and accounts for their interactions through interfacial motions and mass exchanges. Bai & Cheung (2012) transformed a two-layer formulation into an integrated system with separate governing equations for flux- and dispersion-dominated processes. The new governing equations maintain the dispersion characteristics of the conventional two-layer system and without the layer interface enable their implementation for shock-capturing and inundation calculations. We utilize this approach to recast the governing equations of the conventional multi-layer system into a series form that allows reformulation of the vertical velocity and non-hydrostatic terms for direct comparison with the Boussinesq equations and derivation of analytical properties.

We consider a transformation of the flow variables from a multi-layer structure to an integrated system without altering the physical processes. Summation of the flux from each layer gives the depth-averaged horizontal and vertical velocity components in terms of the layer ratio as

$$u = \sum_{i=1}^{N} r_i u_i, \tag{2.26}$$

$$w = \sum_{i=1}^{N} r_i w_i. \tag{2.27}$$

Subtraction of the flux between adjacent layers gives

$$\hat{u}_i = r_i u_i - r_{i+1} u_{i+1}, \quad i = 1, \ldots, N-1 \tag{2.28}$$

$$\hat{w}_i = r_i w_i - r_{i+1} w_{i+1}, \quad i = 1, \ldots, N-1 \tag{2.29}$$

which denote the variation of the velocity across the layer interface. Equations (2.26)–(2.29) map the N layer-averaged velocities (u_i, w_i) into the depth-averaged velocity (u, w) and the velocity variations $(\hat{u}_i, \hat{w}_i)$ across $(N-1)$ interfaces. A positive determinant of $N\prod_{i=1}^{N} r_i$ guarantees a unique linear transformation between the two sets of variables. Inversion of (2.26)–(2.29) gives the layer-averaged velocities

$$u_i = \frac{1}{N r_i}\left[u + \sum_{j=1}^{i-1}(-j)\hat{u}_j + \sum_{j=i}^{N-1}(N-j)\hat{u}_j\right], \quad i = 1, \ldots, N, \tag{2.30}$$

$$w_i = \frac{1}{N r_i}\left[w + \sum_{j=1}^{i-1}(-j)\hat{w}_j + \sum_{j=i}^{N-1}(N-j)\hat{w}_j\right], \quad i = 1, \ldots, N. \tag{2.31}$$

If the lower bound is greater than the upper bound, the term is omitted. It should be noted that the averaged velocity at each layer depends on the depth-averaged velocity and the variations over the entire water column. The flow field defined by these variables is no longer confined within each layer, but is directly connected with the entire system. This feature is more favourable to address the generation and evolution of rotational flows due to abrupt variations of the free surface.

Equations (2.26)–(2.31) allow transformation of the governing equations of the multi-layer system into an equivalent system in terms of the depth-averaged velocity

and the velocity variations over the water column. Summation of the continuity equation (2.23) over the layers from $i = 1$ to N with application of the variable transformation (2.26) gives the continuity equation of the integrated flow as

$$\frac{\partial \zeta}{\partial t} + \frac{\partial hu}{\partial x} = 0. \tag{2.32}$$

This continuity equation is identical to that of the nonlinear shallow-water equations, but different from that of typical Boussinesq formulations. It balances the local acceleration of the surface elevation with the horizontal flux without interference from dispersion and fully conserves mass in discontinuous or dispersive flows. Subtraction of the continuity equations between adjacent layers with the variable transformation (2.28) and implementation of the relative vertical velocity in (2.13) gives the remaining $(N-1)$ continuity equations for the integrated system as

$$\frac{\partial h\hat{u}_i}{\partial x} + 2\Delta w_{z_i} - \Delta w_{z_{i+1}} - \Delta w_{z_{i-1}} + (r_i - r_{i+1})\frac{\partial \zeta}{\partial t} = 0. \tag{2.33}$$

This system of $(N-1)$ equations complements (2.32) to account for the vertical flow structure in the continuity equation (2.23) of the multi-layer flow, which in turn contributes to wave dispersion. For equidistant layers, the term $(r_i - r_{i+1})\,(\partial\zeta/\partial t)$ disappears and the relative vertical velocity at interfaces $(i-1)$, i and $(i+1)$ is balanced by the variation of the flux in the horizontal and vertical directions.

The momentum equations (2.24) and (2.25) of the multi-layer flow are separated into flux- and dispersion-dominated systems through the transformation in (2.26)–(2.31). Summation of the horizontal momentum equations (2.24) over the water column defines the evolution of the depth-averaged horizontal velocity as

$$\begin{aligned}\frac{\partial u}{\partial t} + \frac{\epsilon}{h}\left\{\frac{\partial}{\partial x}\sum_{k=1}^{N}\left[\frac{h}{N^2 r_k}\left(u + \sum_{j=1}^{k-1}(-j)\hat{u}_j + \sum_{j=k}^{N-1}(N-j)\hat{u}_j\right)^2\right] - u\frac{\partial hu}{\partial x}\right\} + \frac{\partial \zeta}{\partial x}\\ + \frac{\mu^2}{h}\left\{\frac{1}{2}\frac{\partial}{\partial x}\left[hr_1(q_d + q_{z_1}) + \sum_{j=2}^{N-1} hr_j(q_{z_{j-1}} + q_{z_j}) + hr_N q_{z_{N-1}}\right] - q_d\frac{\partial d}{\partial x}\right\} = 0.\end{aligned} \tag{2.34}$$

Subtraction of (2.24) between adjacent layers yields $(N-1)$ horizontal momentum equations for the evolution of the velocity profile about its depth-averaged value:

$$\begin{aligned}\frac{\partial \hat{u}_i}{\partial t} + \frac{\epsilon}{h}\left\{\frac{\partial}{\partial x}\left[\frac{h}{N^2 r_i}\left(u + \sum_{j=1}^{i-1}(-j)\hat{u}_j + \sum_{j=i}^{N-1}(N-j)\hat{u}_j\right)^2\right.\right.\\ \left.\left. - \frac{h}{N^2 r_{i+1}}\left(u + \sum_{j=1}^{i}(-j)\hat{u}_j + \sum_{j=i+1}^{N-1}(N-j)\hat{u}_j\right)^2\right] - \hat{u}_i\frac{\partial hu}{\partial x}\right\}\\ + \frac{\mu^2}{h}\left\{\frac{1}{2}\frac{\partial}{\partial x}[hr_i(q_{z_i} + q_{z_{i-1}}) - hr_{i+1}(q_{z_i} + q_{z_{i+1}})]\right.\\ \left. - 2q_{z_i}\frac{\partial z_i}{\partial x} - q_{z_{i+1}}\frac{\partial z_{i+1}}{\partial x} - q_{z_{i-1}}\frac{\partial z_{i-1}}{\partial x}\right\}\\ + \frac{1}{h}\frac{\partial \zeta}{\partial x}(2z_i - z_{i+1} - z_{i-1}) + \frac{2\epsilon}{h}u_{z_i}\Delta w_{z_i} - \frac{\epsilon}{h}u_{z_{i+1}}\Delta w_{z_{i+1}} - \frac{\epsilon}{h}u_{z_{i-1}}\Delta w_{z_{i-1}} = 0.\end{aligned} \tag{2.35}$$

The depth-averaged velocity u and the variations $\hat{u}_i$ across layer interfaces are involved in the advection terms, which play a fundamental role in nonlinear momentum transport in the horizontal direction. Similarly, the vertical momentum equation (2.25) of the multi-layer system is transformed to

$$\frac{\partial w}{\partial t}+\frac{\epsilon}{h}\left\{\frac{\partial}{\partial x}\sum_{k=1}^{N}\left[\frac{h}{N^2 r_k}\left(u+\sum_{j=1}^{k-1}(-j)\hat{u}_j+\sum_{j=k}^{N-1}(N-j)\hat{u}_j\right)\right.\right.$$
$$\left.\left.\times\left(w+\sum_{j=1}^{k-1}(-j)\hat{w}_j+\sum_{j=k}^{N-1}(N-j)\hat{w}_j\right)\right]-w\frac{\partial hu}{\partial x}\right\}-\frac{q_d}{h}=0, \tag{2.36}$$

$$\frac{\partial \hat{w}_i}{\partial t}+\frac{\epsilon}{h}\left\{\frac{\partial}{\partial x}\left[\frac{h}{N^2 r_i}\left(u+\sum_{j=1}^{i-1}(-j)\hat{u}_j+\sum_{j=i}^{N-1}(N-j)\hat{u}_j\right)\right.\right.$$
$$\times\left(w+\sum_{j=1}^{i-1}(-j)\hat{w}_j+\sum_{j=i}^{N-1}(N-j)\hat{w}_j\right)$$
$$-\frac{h}{N^2 r_{i+1}}\left(u+\sum_{j=1}^{i}(-j)\hat{u}_j+\sum_{j=i+1}^{N-1}(N-j)\hat{u}_j\right)$$
$$\left.\left.\times\left(w+\sum_{j=1}^{i}(-j)\hat{w}_j+\sum_{j=i+1}^{N-1}(N-j)\hat{w}_j\right)\right]-\hat{w}_i\frac{\partial hu}{\partial x}\right\}$$
$$+\frac{2q_{z_i}}{h}-\frac{q_{z_{i+1}}}{h}-\frac{q_{z_{i-1}}}{h}+\frac{2\epsilon}{h}w_{z_i}\Delta w_{z_i}-\frac{\epsilon}{h}w_{z_{i+1}}\Delta w_{z_{i+1}}-\frac{\epsilon}{h}w_{z_{i-1}}\Delta w_{z_{i-1}}=0. \tag{2.37}$$

The depth-averaged vertical velocity and the variations over the water column are related to the vertical velocity at the interface by the trapezoidal rule,

$$w=\frac{r_1}{2}(w_d+w_{z_1})+\sum_{j=2}^{N-1}\frac{r_j}{2}(w_{z_{j-1}}+w_{z_j})+\frac{r_N}{2}(w_{z_{N-1}}+w_\zeta), \tag{2.38}$$

$$\hat{w}_i=\frac{r_i}{2}(w_{z_{i-1}}+w_{z_i})-\frac{r_{i+1}}{2}(w_{z_i}+w_{z_{i+1}}), \tag{2.39}$$

where w_ζ and w_d are given by the kinematic boundary conditions at the free surface and bottom in (2.21) and (2.22).

The integrated system defined by (2.32)–(2.37) is equivalent to the governing equations (2.23)–(2.25) of the conventional multi-layer system, but provides separate descriptions of dispersion- and flux-dominated processes. In deep water, the dispersion-dominated governing equations (2.33), (2.35) and (2.37) alter the depth-averaged velocity to describe short-period dispersive waves. As waves propagate into shallow water, the flux-dominated governing equations (2.32), (2.34) and (2.36) describe breaking and broken waves as bores through momentum conservation, and wave runup and drawdown as sheet flows. Bai & Cheung (2012) demonstrated in a two-layer model that the dispersion-dominated system facilitates advection over the water column in shock-related hydraulic processes without creating numerical instabilities. The two sets of governing equations are coupled through the velocity variations ($\hat{u}_i$, $\hat{w}_i$) over the entire water column, in contrast to the conventional multi-layer formulation, in which the interactions only take place at the interfaces. Comparing

with Boussinesq formulations, the integrated system explicitly resolves the vertical flow structure and non-hydrostatic pressure without predefined distributions associated with gravity waves. This enables the description of vertical circulations induced by bottom and free-surface conditions. The governing equations involve only first-order derivatives, which simplifies the numerical procedures and allows implementation of two-way nested grids to improve model efficiency.

Following the approach of Bai (2012), we convert the governing equations of the integrated multi-layer system into a Boussinesq form in terms of high-order derivatives of ζ, u and $\hat{u}_i$. The non-hydrostatic pressure q_d and q_{z_i} can be explicitly expressed in terms of these variables by invoking the interface continuity (2.33), the vertical velocity approximations in (2.38) and (2.39) and the kinematic boundary conditions (2.21) and (2.22). Substitution of the resulting expressions eliminates the non-hydrostatic pressure terms in the horizontal momentum equations (2.34) and (2.35), which together with the continuity equation (2.32) constitute the Boussinesq form of the integrated multi-layer system. The first- and second-order governing equations are then extracted through the perturbation expansion

$$\zeta = \zeta^{(1)} + \epsilon\zeta^{(2)} + \epsilon^2\zeta^{(3)} + \cdots, \tag{2.40}$$

$$u = u^{(1)} + \epsilon u^{(2)} + \epsilon^2 u^{(3)} + \cdots, \tag{2.41}$$

$$\hat{u}_i = \hat{u}_i^{(1)} + \epsilon\hat{u}_i^{(2)} + \epsilon^2\hat{u}_i^{(3)} + \cdots, \tag{2.42}$$

where the superscripts (1), (2) and (3) represent the order of the solution. This allows derivation of linear and nonlinear wave properties for optimization of the layer structure and comparison with those from the Boussinesq equations. The derived wave properties apply specifically to the proposed governing equations (2.32)–(2.37) and their antecedent form defined by (2.23)–(2.25), which reflect a piecewise linear distribution of the velocity profile. Numerical models based directly on the primitive Euler equations, such as Stelling & Zijlema (2003) and Wu *et al.* (2010), would exhibit different wave properties depending on the numerical scheme and the free-surface treatment.

3. Linear wave properties

Waves slow down and shoal as they propagate from deep to shallow water. Linear dispersion, which relates the wave period and water depth to the celerity, is commonly used to measure the performance of coastal wave models. We derive the dispersion relations from the linearized governing equations of the integrated multi-layer systems and the Boussinesq equations for comparison with the exact solution from Airy wave theory. Since all the terms are of the same order of magnitude, the governing equations are written in dimensional form for a direct comparison.

3.1. *Governing equations*

Substitution of the perturbation expansions (2.40)–(2.42) into the Boussinesq form of the integrated multi-layer system decomposes the governing equations by an order of magnitude in terms of ϵ. After dropping the nonlinear terms, the linearized governing equations for the one-layer system are

$$\frac{\partial\zeta^{(1)}}{\partial t} + d\frac{\partial u^{(1)}}{\partial x} = 0, \tag{3.1}$$

$$\frac{\partial u^{(1)}}{\partial t} + g\frac{\partial\zeta^{(1)}}{\partial x} - \frac{d^2}{4}\frac{\partial^3 u^{(1)}}{\partial x^2\partial t} = 0. \tag{3.2}$$

The system includes a continuity and a momentum equation and describes weakly dispersive flows through a third-order derivative of the depth-averaged horizontal velocity. The two-layer system involves one adjustable interface to enhance the dispersion properties. The corresponding governing equations are

$$\frac{\partial \zeta^{(1)}}{\partial t} + d\frac{\partial u^{(1)}}{\partial x} = 0, \tag{3.3}$$

$$\frac{\partial u^{(1)}}{\partial t} + g\frac{\partial \zeta^{(1)}}{\partial x} + \frac{d^2}{16}(r_1^2 - 8r_1r_2 - 5r_2^2 - 3r_1 - r_2)\frac{\partial^3 u^{(1)}}{\partial x^2 \partial t} + \frac{d^2}{16}(r_1^2 - r_2^2 - 3r_1 - r_2)\frac{\partial^3 \hat{u}_1^{(1)}}{\partial x^2 \partial t} = 0, \tag{3.4}$$

$$\frac{\partial \hat{u}_1^{(1)}}{\partial t} + \frac{d^2}{16}(r_1^2 - 10r_1r_2 + 5r_2^2 - 3r_1 + r_2)\frac{\partial^3 u^{(1)}}{\partial x^2 \partial t} + \frac{d^2}{16}(r_1^2 - 2r_1r_2 + r_2^2 - 3r_1 + r_2)\frac{\partial^3 \hat{u}_1^{(1)}}{\partial x^2 \partial t} = 0. \tag{3.5}$$

Comparing with the one-layer system, a second momentum equation (3.5) describes dispersion-dominated processes through evolution of $\hat{u}_1$, which is coupled with the depth-averaged velocity via the momentum equation (3.4). The three-layer system includes a third momentum equation in the governing equations, which read

$$\frac{\partial \zeta^{(1)}}{\partial t} + d\frac{\partial u^{(1)}}{\partial x} = 0, \tag{3.6}$$

$$\frac{\partial u^{(1)}}{\partial t} + g\frac{\partial \zeta^{(1)}}{\partial x} + \frac{d^2}{12}(-r_1^2 - 3r_2^2 - 5r_3^2 - 6r_1r_2 - 10r_2r_3 - 10r_1r_3)\frac{\partial^3 u^{(1)}}{\partial x^2 \partial t} + \frac{d^2}{12}(-2r_1^2 - 3r_2^2 - r_3^2 - 6r_1r_2 - 2r_2r_3 - 2r_1r_3)\frac{\partial^3 \hat{u}_1^{(1)}}{\partial x^2 \partial t} + \frac{d^2}{12}(-r_1^2 - 3r_2^2 - 2r_3^2 - 6r_1r_2 - 4r_2r_3 - 4r_1r_3)\frac{\partial^3 \hat{u}_2^{(1)}}{\partial x^2 \partial t} = 0, \tag{3.7}$$

$$\frac{\partial \hat{u}_1^{(1)}}{\partial t} + (r_1 - r_2)\, g\frac{\partial \zeta^{(1)}}{\partial x} + \frac{d^2}{12}(-r_1^2 + 3r_2^2 - 6r_1r_2 + 10r_2r_3 - 10r_1r_3)\frac{\partial^3 u^{(1)}}{\partial x^2 \partial t} + \frac{d^2}{12}(-2r_1^2 + 3r_2^2 - 6r_1r_2 + 2r_2r_3 - 2r_1r_3)\frac{\partial^3 \hat{u}_1^{(1)}}{\partial x^2 \partial t} + \frac{d^2}{12}(-r_1^2 + 3r_2^2 - 6r_1r_2 + 4r_2r_3 - 4r_1r_3)\frac{\partial^3 \hat{u}_2^{(1)}}{\partial x^2 \partial t} = 0, \tag{3.8}$$

$$\frac{\partial \hat{u}_2^{(1)}}{\partial t} + (r_1 + 2r_2 - 1)\, g\frac{\partial \zeta^{(1)}}{\partial x} + \frac{d^2}{12}(-3r_2^2 + 5r_3^2 - 10r_2r_3)\frac{\partial^3 \hat{u}^{(1)}}{\partial x^2 \partial t} + \frac{d^2}{12}(-3r_2^2 + r_3^2 - 2r_2r_3)\frac{\partial^3 \hat{u}_1^{(1)}}{\partial x^2 \partial t} + \frac{d^2}{12}(-3r_2^2 + 2r_3^2 - 4r_2r_3)\frac{\partial^3 \hat{u}_2^{(1)}}{\partial x^2 \partial t} = 0. \tag{3.9}$$

Different from the two-layer system, the spatial derivative of the surface elevation can influence the velocity profile through the momentum equations (3.8) and (3.9). The coefficients of the third-order derivatives in the two- and three-layer systems

are composed of second-degree polynomials with one and two free parameters for adjustment of the interfaces and modification of the dispersion properties.

The integrated multi-layer systems in the Boussinesq form have the same continuity equation and share the same structure in the momentum equations. Each additional layer introduces a momentum equation for the corresponding velocity variation, which in turn is coupled with the depth-averaged horizontal velocity to better resolve the profile and consequently the dispersion properties, but the highest order of derivatives remains at three. In contrast, the Boussinesq equations improve the dispersion properties through increasing order of the horizontal velocity derivative with predefined profile characteristics. For comparison, we consider the linearized Boussinesq equations from Nwogu (1993),

$$\frac{\partial \zeta^{(1)}}{\partial t} + d\frac{\partial u^{(1)}}{\partial x} + \left(\alpha + \frac{1}{3}\right) d^3 \frac{\partial^3 u^{(1)}}{\partial x^3} = 0, \tag{3.10}$$

$$\frac{\partial u^{(1)}}{\partial t} + g\frac{\partial \zeta^{(1)}}{\partial x} + \alpha\, d^2 \frac{\partial^3 u^{(1)}}{\partial x^2 \partial t} = 0, \tag{3.11}$$

where $u^{(1)}$ is the horizontal velocity defined at an elevation adjustable by the free parameter α. The governing equations reduce to the linearized classical Boussinesq equations of Peregrine (1967) for $\alpha = -1/3$ and the same structure as the one-layer system defined by (3.1) and (3.2). Gobbi *et al.* (2000) utilized two velocity potentials defined at different elevations adjustable by the free parameters B and D. The linearized governing equations are rewritten in terms of the horizontal velocity as

$$\frac{\partial \zeta^{(1)}}{\partial t} + d\frac{\partial u^{(1)}}{\partial x} + \frac{d^3}{2}\left(B - \frac{1}{3}\right)\frac{\partial^3 u^{(1)}}{\partial x^3} + \frac{d^5}{4}\left(B^2 - \frac{B}{3} - \frac{D}{6} + \frac{1}{30}\right)\frac{\partial^5 u^{(1)}}{\partial x^5} = 0, \tag{3.12}$$

$$\frac{\partial u^{(1)}}{\partial t} + g\frac{\partial \zeta^{(1)}}{\partial x} + \frac{d^2}{2}(B-1)\frac{\partial^3 u^{(1)}}{\partial x^2 \partial t} + \frac{d^4}{4}\left(B^2 - B - \frac{D}{6} + \frac{1}{6}\right)\frac{\partial^5 u^{(1)}}{\partial x^4 \partial t} = 0. \tag{3.13}$$

Similar to the approach of Nwogu (1993), the free parameters allow for tuning of the dispersion properties. The highest order of derivatives increases from three to five associated with the improvement in dispersion.

The Boussinesq and multi-layer approaches stem from the same root. The linearized classical Boussinesq equations and one-layer system possess the same structure with derivatives of up to third-order derived from depth integration of a linear velocity profile. Subsequent extensions of the Boussinesq approach by Nwogu (1993) and Gobbi *et al.* (2000) provide additional degrees of freedom in defining a continuous velocity profile, which results in higher-order derivatives in both the momentum and continuity equations. In contrast, the multi-layer approach resolves the velocity profile by a piecewise linear distribution while maintaining the highest order of the derivatives at three and the same continuity equation as the classical Boussinesq equations.

3.2. *Dispersion relations*

Linear dispersion is a characteristic property defining wave propagation in water of constant depth. Substitution of a system of small-amplitude progressive waves with wavenumber k and angular frequency ω into the linearized governing equations gives rise to the corresponding dispersion relations for comparison with the exact relation from Airy wave theory,

$$c_{Airy}^2 = gd\frac{\tanh(kd)}{kd}, \tag{3.14}$$

where kd denotes the water depth parameter. The one-layer, two-layer and three-layer systems give the dispersion relations as

$$c_1^2 = \frac{gd}{1 + \frac{1}{4}k^2d^2}, \tag{3.15}$$

$$c_2^2 = gd\frac{1 + \beta_1 k^2 d^2}{1 + \beta_2 k^2 d^2 + \beta_3 k^4 d^4}, \tag{3.16}$$

$$c_3^2 = gd\frac{1 + \gamma_1 k^2 d^2 + \gamma_2 k^4 d^4}{1 + \gamma_3 k^2 d^2 + \gamma_4 k^4 d^4 + \gamma_5 k^6 d^6}, \tag{3.17}$$

in which the coefficients describing the structure of the two-layer system are given as

$$\beta_1 = -\tfrac{1}{16}(r_1^2 - 2r_1r_2 + r_2^2 - 3r_1 + r_2), \tag{3.18}$$

$$\beta_2 = +\tfrac{1}{32}(-4r_1^2 + 20r_1r_2 + 8r_2^2 + 12r_1), \tag{3.19}$$

$$\beta_3 = +\tfrac{1}{32}(r_1^2r_2^2 - r_1r_2^3 + r_1r_2^2), \tag{3.20}$$

and for the three-layer system as

$$\begin{aligned}\gamma_1 = &-\tfrac{1}{16}(+4r_1^3 + 16r_1^2r_2 + 8r_1^2r_3 + 16r_1r_2^2 + 16r_1r_2r_3 + 4r_1r_3^2 + 4r_2^3 \\ &+ 8r_2^2r_3 + 4r_2r_3^2 - 4r_1^2 - 16r_1r_2 - 8r_1r_3 - 4r_2^2 - 8r_2r_3),\end{aligned} \tag{3.21}$$

$$\begin{aligned}\gamma_2 = &-\tfrac{1}{16}(+r_1^3r_2{}^2 + 2r_1^3r_2r_3 + r_1^2r_2^3 + 4r_1^2r_2^2r_3 + r_1^2r_2r_3^2 + 2r_1r_2^3r_3 \\ &+ r_1r_2^2r_3^2 - r_1^2r_2^2 - 2r_1^2r_2r_3 - 2r_1r_2^2r_3),\end{aligned} \tag{3.22}$$

$$\gamma_3 = +\tfrac{1}{64}(16r_1^2 + 64r_1r_2 + 64r_1r_3 + 16r_2^2 + 64r_2r_3 + 16r_3^2), \tag{3.23}$$

$$\gamma_4 = +\tfrac{1}{64}(4r_1^2r_2^2 + 16r_1^2r_2r_3 + 4r_1^2r_3^2 + 16r_1r_2^2r_3 + 16r_1r_2r_3^2 + 4r_2^2r_3^2), \tag{3.24}$$

$$\gamma_5 = +\tfrac{1}{64}r_1^2r_2^2r_3^2. \tag{3.25}$$

The dispersion relations of the one-, two- and three-layer systems are rational functions of the depth parameter kd in the form of $[0, 2]$, $[2, 4]$ and $[4, 6]$ Padé expansions of the exact dispersion relation (3.14). This indicates relatively rapid convergence in terms of a $[2N - 2, 2N]$ Padé expansion for an N-layer system. The layer arrangement, which modifies the coefficients of the expansion, can be optimized for further enhancement.

The linear dispersion properties of the Boussinesq approach have been examined extensively in the literature. The linearized Boussinesq equations of Peregrine (1967) obtained by setting $\alpha = -1/3$ in (3.10) and (3.11), Nwogu (1993) with $\alpha = -0.4$, and Gobbi *et al.* (2000) with optimized values of $B = 1/9$ and $D = 5/189$ in (3.12) and (3.13) give the dispersion relations as

$$c_{PG}^2 = \frac{gd}{1 + \frac{1}{3}k^2d^2}, \tag{3.26}$$

$$c_{NG}^2 = gd\frac{1 + \frac{1}{15}k^2d^2}{1 + \frac{2}{5}k^2d^2}, \tag{3.27}$$

$$c_{GB}^2 = gd\frac{1 + \frac{1}{9}k^2d^2 + \frac{1}{945}k^4d^4}{1 + \frac{4}{9}k^2d^2 + \frac{1}{63}k^4d^4}, \tag{3.28}$$

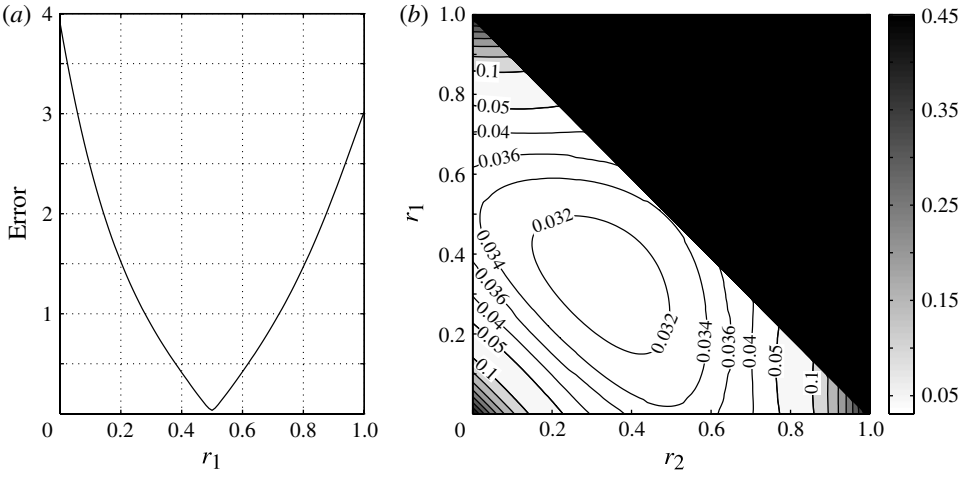

FIGURE 2. Relative errors for the (*a*) two-layer and (*b*) three-layer systems as functions of layer ratios.

which correspond to [0, 2], [2, 2] and [4, 4] Padé expansions. The dispersion relation (3.26) of the classical Boussinesq equations contains the same polynomial as the one-layer system (3.15), but with a slightly different coefficient carried over from the governing equations. Both provide basic approximations to the exact dispersion relation for small values of kd. The dispersion properties improve with increasing resolution of the flow structure through high-order terms in the governing equations. In general, the Boussinesq approach gives rise to a $[2L, 2M]$ Padé approximation associated with the highest odd-order derivative of $(2L + 1)$ and $(2M + 1)$ in the continuity and momentum equations. The multi-layer approach does not explicitly curtail high-order terms in the governing equations. The $[2N-2, 2N]$ Padé convergence characteristics of an N-layer system results from the assumed linear distribution of the velocity in each layer as inferred from the analysis of Lynett & Liu (2004*a*,*b*).

Analogous to the free parameters α in Nwogu (1993) and B and D in Gobbi *et al.* (2000), the layer arrangement allows optimization of the dispersion relations through r_1 and (r_1, r_2) for the two- and three-layer systems. The relative error is computed over $0.01 \leqslant kd \leqslant 6$ to account for a wide spectrum of ocean waves,

$$\text{error} = \int_{0.01}^{6} \left| \frac{c_N^2}{c_{Airy}^2} - 1 \right| \mathrm{d}(kd). \tag{3.29}$$

Figure 2 shows the computed error as a function of r_1 and (r_1, r_2) for the two- and three-layer systems. The optimal elevation of the interface for the two-layer model is at mid-flow depth ($r_1 = 0.5$). This equidistant layer arrangement gives a minimum error of 0.034 45. Moving the interface either to the surface or to the bottom will sharply increase the error. The equidistant arrangement with $r_1 = r_2 = 1/3$ in the three-layer system also yields a relatively low error of 0.0310 versus the minimum error of 0.0309 for the optimal arrangement of $r_1 = 0.32$ and $r_2 = 0.39$. The results show relatively stable convergence of the solution and the error is not sensitive to (r_1, r_2) around the optimal arrangement. Since the equidistant arrangement can produce reliable estimates of the celerity, we adopt $r_1 = 1/2$ in the two-layer system

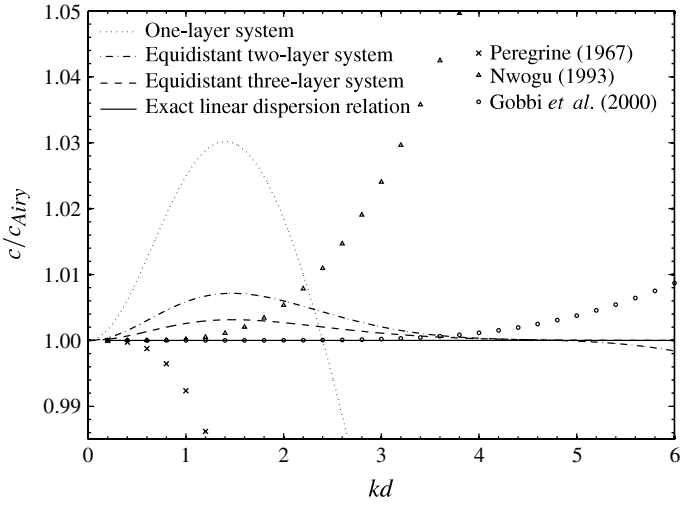

FIGURE 3. Normalized wave celerity from multi-layer and Boussinesq models.

and $r_1 = r_2 = 1/3$ in the three-layer system to give

$$c_2^2 = gd\frac{1 + \frac{1}{16}k^2d^2}{1 + \frac{3}{8}k^2d^2 + \frac{1}{256}k^4d^4}, \tag{3.30}$$

$$c_3^2 = gd\frac{1 + \frac{5}{54}k^2d^2 + \frac{1}{1296}k^4d^4}{1 + \frac{5}{12}k^2d^2 + \frac{5}{432}k^4d^4 + \frac{1}{46\,656}k^6d^6}. \tag{3.31}$$

Equations (3.30) and (3.31) share similar coefficients with the respective terms in the dispersion relations (3.27) and (3.28) from Nwogu (1993) and Gobbi *et al.* (2000), but include higher-order terms in the denominator that would become important for large values of kd.

Figure 3 compares the dispersion relations from the multi-layer and Boussinesq approaches in terms of the celerity normalized by the exact solution. The $[0, 2]$ Padé expansion of Peregrine (1967) gives a good approximation of wave dispersion in shallow water, but diverges rapidly with large values of kd. An improvement of the horizontal velocity distribution from linear to quadratic by Nwogu (1993) leads to improved convergence at $[2, 2]$ with a good approximation of wave dispersion in $0 \leqslant kd \leqslant 3$. The computed celerity closely follows the exact linear dispersion for $0 \leqslant kd \leqslant 1$ and gives a relative error of 2.4 % at $kd = 3$, but diverges with larger values of kd. The $[4, 4]$ Padé expansion from Gobbi *et al.* (2000) is almost identical to the exact solution in the range $0 \leqslant kd \leqslant 3.6$ and produces a small error of about 1 % at $kd = 6$. While the solutions from the Boussinesq models converge asymptotically in shallow water, the multi-layer solutions show a different convergence pattern, with positive gradients at $kd = 0$. The one-layer solution reaches a local peak error of 3 % in intermediate water depth before diverging in deep water. The two- and three-layer models slightly overestimate the celerity by up to 0.7 and 0.3 % in $0 \leqslant kd \leqslant 3.6$, but provide better agreement for larger values of kd. Figure 4 highlights the convergence characteristics by plotting the celerity of the one-, two- and three-layer models up to $kd = 24$. The one-layer model follows the same pattern as Peregrine (1967) for large values of kd, since both involve depth integration of the horizontal velocity with an

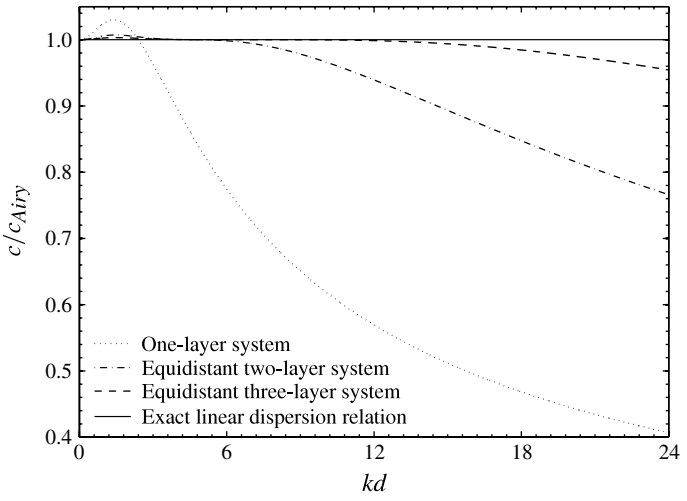

FIGURE 4. Convergence of normalized wave celerity from multi-layer models.

assumed linear distribution that leads to a [0, 2] Padé expansion. Each additional layer increases the order of the Padé expansion by [2, 2]. The celerity from the two-layer model has a small error of $-0.16\,\%$ at $kd = 6$, while the three-layer model closely follows the exact solution. Both solutions diverge monotonically with larger values of kd. The comparison indicates that the multi-layer approach provides reasonable approximations of the dispersion in shallow and intermediate water depth but is much more robust in deep water than Boussinesq models with comparable orders of Padé expansion.

4. Nonlinear wave properties

Dispersion defines basic coastal wave transformation over varying bathymetry. The free-surface and flow advection are nonlinear, leading to further modifications of the waveform and velocity profile. Nonlinearity transfers energy to high- and low-frequency components in the generation of forced short and long waves. This section summarizes the development of the second-order governing equations for the one-, two- and three-layer systems in dimensional form and examines different optimization strategies for the two- and three-layer systems. The second-order governing equations of the multi-layer approach allow derivation of quadratic transfer functions for comparison with the corresponding solutions from the Boussinesq equations and second-order Stokes wave theory.

4.1. *Second-order governing equations*

The second-order governing equations account for the nonlinear interactions, which provide a correction to the linear solution. The non-homogeneous equations have the same structure as the linear governing equations, but with the addition of nonlinear forcing terms on the right-hand side. After implementation of the perturbation expansions (2.40)–(2.42) in the multi-layer system, collection of terms with leading order of ϵ provides the second-order governing equations. For the one-layer system,

we have

$$\frac{\partial \zeta^{(2)}}{\partial t} + d\frac{\partial u^{(2)}}{\partial x} = -\frac{\partial \zeta^{(1)}}{\partial x}u^{(1)} - \zeta^{(1)}\frac{\partial u^{(1)}}{\partial x}, \tag{4.1}$$

$$\begin{aligned}\frac{\partial u^{(2)}}{\partial t} + g\frac{\partial \zeta^{(2)}}{\partial x} - \frac{d^2}{4}\frac{\partial^3 u^{(2)}}{\partial x^2 \partial t} &= -u^{(1)}\frac{\partial u^{(1)}}{\partial x} + \frac{d^2}{4}\frac{\partial u^{(1)}}{\partial x}\frac{\partial^2 u^{(1)}}{\partial x^2} + \frac{d^2 u^{(1)}}{4}\frac{\partial^3 u^{(1)}}{\partial x^3} \\ &\quad + \frac{d\zeta^{(1)}}{4}\frac{\partial^3 u^{(1)}}{\partial x^2 \partial t} + \frac{d}{4}\frac{\partial \zeta^{(1)}}{\partial x}\frac{\partial^2 u^{(1)}}{\partial x \partial t} - \frac{d}{4}\frac{\partial^2 \zeta^{(1)}}{\partial x^2}\frac{\partial u^{(1)}}{\partial t},\end{aligned} \tag{4.2}$$

which contain the basic nonlinear forcing from the non-hydrostatic formulation. The forcing terms in the continuity equation (4.1) account for nonlinearity associated with the free-surface motion. The momentum equation (4.2) contains six forcing terms that constitute the fundamental structure of the multi-layer system. The first term $u\,\partial u/\partial x$, which comes from nonlinear advection of the depth-averaged velocity, does not influence dispersion processes. The remaining terms with high-order derivatives, $(\partial u/\partial x)(\partial^2 u/\partial x^2)$, $u\,\partial^3 u/\partial x^3$, $(\partial \zeta/\partial x)(\partial^2 u/\partial x\,\partial t)$, $\zeta\,\partial^3 u/\partial x^2\,\partial t$ and $(\partial u/\partial t)(\partial^2 \zeta/\partial x^2)$, arise from coupling between nonlinearity and dispersion. The absence of adjustable vertical flow structures in the governing equations of the one-layer system implies a low-order approximation of dispersion that in turn might restrict the model's capability to describe nonlinear processes.

Introduction of one interface over the water column provides a degree of freedom in describing the vertical flow structure through the velocity variation $\hat{u}_1$. This results in a third governing equation and modification of the forcing terms. For demonstration, we present the second-order governing equations for the two-layer system with an equidistant layer arrangement. The continuity equation reads

$$\frac{\partial \zeta^{(2)}}{\partial t} + d\frac{\partial u^{(2)}}{\partial x} = -\frac{\partial \zeta^{(1)}}{\partial x}u^{(1)} - \zeta^{(1)}\frac{\partial u^{(1)}}{\partial x}. \tag{4.3}$$

The two-layer system gives rise to separate momentum equations for flux- and dispersion-dominated processes, respectively, as

$$\begin{aligned}&\frac{\partial u^{(2)}}{\partial t} + g\frac{\partial \zeta^{(2)}}{\partial x} - \frac{5d^2}{16}\frac{\partial^3 u^{(2)}}{\partial x^2 \partial t} - \frac{d^2}{8}\frac{\partial^3 \hat{u}_1^{(2)}}{\partial x^2 \partial t} \\ &\quad = -u^{(1)}\frac{\partial u^{(1)}}{\partial x} - 2\hat{u}_1^{(1)}\frac{\partial \hat{u}_1^{(1)}}{\partial x} + d^2 u^{(1)}\frac{\partial^3}{\partial x^3}\left(\frac{u^{(1)}}{2} + \frac{\hat{u}_1^{(1)}}{8}\right) - d^2\hat{u}_1^{(1)}\frac{\partial^3}{\partial x^3}\left(\frac{9u^{(1)}}{16} + \frac{\hat{u}_1^{(1)}}{16}\right) \\ &\qquad - d^2\frac{\partial u^{(1)}}{\partial x}\frac{\partial^2}{\partial x^2}\left(\frac{\hat{u}_1^{(1)}}{8} - \frac{u^{(1)}}{4}\right) + d^2\frac{\partial \hat{u}_1^{(1)}}{\partial x}\frac{\partial^2}{\partial x^2}\left(\frac{\hat{u}_1^{(1)}}{16} - \frac{13u^{(1)}}{16}\right) \\ &\qquad + d\zeta^{(1)}\frac{\partial^3}{\partial x^2 \partial t}\left(\frac{\hat{u}_1^{(1)}}{4} + \frac{7u^{(1)}}{16}\right) + d\frac{\partial \zeta^{(1)}}{\partial x}\frac{\partial^2}{\partial x \partial t}\left(\frac{9u^{(1)}}{16} + \frac{11\hat{u}_1^{(1)}}{16}\right) \\ &\qquad + d\,\frac{\partial^2 \zeta^{(1)}}{\partial x^2}\frac{\partial}{\partial t}\left(\frac{5\hat{u}_1^{(1)}}{16} - \frac{3u^{(1)}}{16}\right),\end{aligned} \tag{4.4}$$

$$\begin{aligned}&\frac{\partial \hat{u}_1^{(2)}}{\partial t} - \frac{d^2}{8}\frac{\partial^3 u^{(2)}}{\partial x^2 \partial t} - \frac{d^2}{16}\frac{\partial^3 \hat{u}_1^{(2)}}{\partial x^2 \partial t} \\ &\quad = -\hat{u}_1^{(1)}\frac{\partial u^{(1)}}{\partial x} - u^{(1)}\frac{\partial \hat{u}_1^{(1)}}{\partial x} + d\frac{\zeta^{(1)}\partial^3}{\partial x^2 \partial t}\left(\frac{3u^{(1)}}{16} + \frac{\hat{u}_1^{(1)}}{8}\right)\end{aligned}$$

$$+d\frac{\partial\zeta^{(1)}}{\partial x}\frac{\partial^2}{\partial x\,\partial t}\left(\frac{3\hat{u}_1^{(1)}}{16}-\frac{u^{(1)}}{8}\right)-d\frac{\partial^2\zeta^{(1)}}{\partial x^2}\frac{\partial}{\partial t}\left(\frac{u^{(1)}}{16}-\frac{\hat{u}_1^{(1)}}{8}\right)$$
$$+d^2\frac{u^{(1)}}{16}\frac{\partial^3\hat{u}_1^{(1)}}{\partial x^3}+d^2\frac{3u^{(1)}}{16}\frac{\partial^3u^{(1)}}{\partial x^3}-d^2\frac{3\hat{u}_1^{(1)}}{16}\frac{\partial^3u^{(1)}}{\partial x^3}$$
$$+\frac{d^2}{16}\frac{\partial u^{(1)}}{\partial x}\frac{\partial^2u^{(1)}}{\partial x^2}-\frac{5d^2}{16}\frac{\partial^2u^{(1)}}{\partial x^2}\frac{\partial\hat{u}_1^{(1)}}{\partial x}-\frac{d^2}{16}\frac{\partial u^{(1)}}{\partial x}\frac{\partial^2\hat{u}_1^{(1)}}{\partial x^2}. \tag{4.5}$$

The continuity equation (4.3) remains the same, while the six sets of forcing terms in the momentum equations (4.4) and (4.5) include contributions from the vertical flow structure. These two momentum equations couple not only in the homogeneous part to improve dispersion but also in the nonlinear forcing to include the effects of vorticity through variation of the velocity over the water column.

A three-layer system includes $\hat{u}_1$ and $\hat{u}_2$ to define the vertical flow structure and two additional momentum equations for the accompanying dispersion processes. The continuity equation remains the same as

$$\frac{\partial\zeta^{(2)}}{\partial t}+d\frac{\partial u^{(2)}}{\partial x}=-\frac{\partial\zeta^{(1)}}{\partial x}u^{(1)}-\zeta^{(1)}\frac{\partial u^{(1)}}{\partial x}. \tag{4.6}$$

For an equidistant layer arrangement, the momentum equation for flux-dominated processes becomes

$$\frac{\partial u^{(2)}}{\partial t}+g\frac{\partial\zeta^{(2)}}{\partial x}-\frac{35d^2}{108}\frac{\partial^3u^{(2)}}{\partial x^2\,\partial t}-\frac{4d^2}{27}\frac{\partial^3\hat{u}_1^{(2)}}{\partial x^2\,\partial t}-\frac{5d^2}{27}\frac{\partial^3\hat{u}_2^{(2)}}{\partial x^2\,\partial t}$$
$$=-\hat{u}_1^{(1)}\frac{\partial}{\partial x}(2\hat{u}_2^{(1)}+4\hat{u}_1^{(1)})-u^{(1)}\frac{\partial u^{(1)}}{\partial x}-\hat{u}_2^{(1)}\frac{\partial}{\partial x}(2\hat{u}_1^{(1)}+4\hat{u}_2^{(1)})$$
$$+d\frac{\partial\zeta^{(1)}}{\partial x}\frac{\partial^2}{\partial x\,\partial t}\left(\frac{19\hat{u}_2^{(1)}}{18}+\frac{35u^{(1)}}{36}+\frac{31\hat{u}_1^{(1)}}{36}\right)+d^2\frac{\partial^2\zeta^{(1)}}{\partial x^2}\frac{\partial}{\partial t}\left(\frac{5\hat{u}_1^{(1)}}{12}+\frac{\hat{u}_2^{(1)}}{2}\right)$$
$$+d\frac{\zeta^{(1)}\partial^3}{\partial x^2\,\partial t}\left(\frac{8\hat{u}_1^{(1)}}{27}+\frac{10\hat{u}_2^{(1)}}{27}+\frac{35u^{(1)}}{54}\right)+d^2u^{(1)}\frac{\partial^3}{\partial x^3}\left(\frac{35u^{(1)}}{108}+\frac{4\hat{u}_1^{(1)}}{27}+\frac{5\hat{u}_2^{(1)}}{27}\right)$$
$$-d^2\hat{u}_1^{(1)}\frac{\partial^3}{\partial x^3}\left(\frac{5\hat{u}_1^{(1)}}{54}+\frac{17\hat{u}_2^{(1)}}{108}+\frac{77u^{(1)}}{108}\right)-d^2\hat{u}_2^{(1)}\frac{\partial^3}{\partial x^3}\left(\frac{5\hat{u}_2^{(1)}}{54}-\frac{\hat{u}_1^{(1)}}{108}+\frac{47u^{(1)}}{54}\right)$$
$$-d^2\frac{\partial u^{(1)}}{\partial x}\frac{\partial^2}{\partial x^2}\left(\frac{4\hat{u}_1^{(1)}}{27}+\frac{5\hat{u}_2^{(1)}}{27}+\frac{35u^{(1)}}{108}\right)-d^2\frac{\partial\hat{u}_1^{(1)}}{\partial x}\frac{\partial^2}{\partial x^2}\left(\frac{109u^{(1)}}{108}-\frac{5\hat{u}_1^{(1)}}{54}+\frac{\hat{u}_2^{(1)}}{108}\right)$$
$$-d^2\frac{\partial\hat{u}_2^{(1)}}{\partial x}\frac{\partial^2}{\partial x^2}\left(\frac{67u^{(1)}}{54}-\frac{5\hat{u}_2^{(1)}}{54}-\frac{17\hat{u}_1^{(1)}}{108}\right). \tag{4.7}$$

The evolution of the vertical flow structure in terms of $\hat{u}_1$ and $\hat{u}_2$ defines dispersion-dominated processes through the momentum equations

$$\frac{\partial\hat{u}_1^{(2)}}{\partial t}-\frac{d^2}{27}\frac{\partial^3u^{(2)}}{\partial x^2\,\partial t}-\frac{5d^2}{108}\frac{\partial^3\hat{u}_1^{(2)}}{\partial x^2\,\partial t}-\frac{d^2}{27}\frac{\partial^3\hat{u}_2^{(2)}}{\partial x^2\,\partial t}$$
$$=-u^{(1)}\frac{\partial\hat{u}_1^{(1)}}{\partial x}-\hat{u}_2^{(1)}\frac{\partial}{\partial x}\left(\frac{\hat{u}_1^{(1)}}{2}+\hat{u}_2^{(1)}\right)$$

$$
\begin{aligned}
&- \hat{u}_1^{(1)} \frac{\partial}{\partial x}(\hat{u}_2^{(1)} + \hat{u}_1^{(1)} + u^{(1)}) + d \frac{\partial \zeta^{(1)}}{\partial x} \frac{\partial^2}{\partial x\, \partial t} \left(\frac{\hat{u}_1^{(1)}}{12} + \frac{\hat{u}_2^{(1)}}{36} \right) \\
&+ d \frac{\partial^2 \zeta^{(1)}}{\partial x^2} \frac{\partial}{\partial t} \left(\frac{\hat{u}_1^{(1)}}{18} + \frac{\hat{u}_2^{(1)}}{36} \right) + d\zeta^{(1)} \frac{\partial^3}{\partial x^2\, \partial t} \left(\frac{5\hat{u}_1^{(1)}}{54} + \frac{2\hat{u}_2^{(1)}}{27} + \frac{2u^{(1)}}{27} \right) \\
&+ d^2 u^{(1)} \frac{\partial^3}{\partial x^3} \left(\frac{u^{(1)}}{27} + \frac{5\hat{u}_1^{(1)}}{108} + \frac{\hat{u}_2^{(1)}}{27} \right) + d^2 \hat{u}_1^{(1)} \frac{\partial^3}{\partial x^3} \left(\frac{\hat{u}_1^{(1)}}{108} - \frac{\hat{u}_2^{(1)}}{108} - \frac{7u^{(1)}}{108} \right) \\
&+ d^2 \hat{u}_2^{(1)} \frac{\partial^3}{\partial x^3} \left(\frac{\hat{u}_2^{(1)}}{27} + \frac{5\hat{u}_1^{(1)}}{108} + \frac{u^{(1)}}{108} \right) - d^2 \frac{\partial u^{(1)}}{\partial x} \frac{\partial^2}{\partial x^2} \left(\frac{5\hat{u}_1^{(1)}}{108} + \frac{\hat{u}_2^{(1)}}{27} + \frac{u^{(1)}}{27} \right) \\
&- d^2 \frac{\partial \hat{u}_1^{(1)}}{\partial x} \frac{\partial^2}{\partial x^2} \left(\frac{17u^{(1)}}{108} + \frac{\hat{u}_1^{(1)}}{108} + \frac{5\hat{u}_2^{(1)}}{108} \right) - d^2 \frac{\partial \hat{u}_2^{(1)}}{\partial x} \frac{\partial^2}{\partial x^2} \left(\frac{7u^{(1)}}{108} + \frac{\hat{u}_2^{(1)}}{27} - \frac{\hat{u}_1^{(1)}}{108} \right),
\end{aligned}
\tag{4.8}
$$

$$
\begin{aligned}
&\frac{\partial \hat{u}_2^{(2)}}{\partial t} - \frac{2d^2}{27} \frac{\partial^3 u^{(2)}}{\partial x^2\, \partial t} - \frac{d^2}{27} \frac{\partial^3 \hat{u}_1^{(2)}}{\partial x^2\, \partial t} - \frac{5d^2}{108} \frac{\partial^3 \hat{u}_2^{(2)}}{\partial x^2\, \partial t} \\
&\quad = -u^{(1)} \frac{\partial \hat{u}_2^{(1)}}{\partial x} + \hat{u}_1^{(1)} \frac{\partial}{\partial x} \left(\frac{\hat{u}_2^{(1)}}{2} - \hat{u}_1^{(1)} \right) \\
&\qquad + \hat{u}_2^{(1)} \frac{\partial}{\partial x}(\hat{u}_1^{(1)} + \hat{u}_2^{(1)} - u^{(1)}) + d \frac{\partial \zeta^{(1)}}{\partial x} \frac{\partial^2}{\partial x\, \partial t} \left(\frac{7\hat{u}_2^{(1)}}{36} + \frac{5\hat{u}_1^{(1)}}{24} \right) \\
&\qquad + d \frac{\partial^2 \zeta^{(1)}}{\partial x^2} \frac{\partial}{\partial t} \left(\frac{7\hat{u}_1^{(1)}}{72} + \frac{\hat{u}_2^{(1)}}{9} \right) + d\zeta^{(1)} \frac{\partial^3}{\partial x^2\, \partial t} \left(\frac{2\hat{u}_1^{(1)}}{27} + \frac{5\hat{u}_2^{(1)}}{54} + \frac{4u^{(1)}}{27} \right) \\
&\qquad + d^2 u^{(1)} \frac{\partial^3}{\partial x^3} \left(\frac{2u^{(1)}}{27} + \frac{\hat{u}_1^{(1)}}{27} + \frac{5\hat{u}_2^{(1)}}{108} \right) - d^2 \hat{u}_1^{(1)} \frac{\partial^3}{\partial x^3} \left(\frac{\hat{u}_1^{(1)}}{27} + \frac{5\hat{u}_2^{(1)}}{108} + \frac{37u^{(1)}}{216} \right) \\
&\qquad - d^2 \hat{u}_2^{(1)} \frac{\partial^3}{\partial x^3} \left(\frac{\hat{u}_2^{(1)}}{108} - \frac{\hat{u}_1^{(1)}}{108} + \frac{19u^{(1)}}{108} \right) - d^2 \frac{\partial u^{(1)}}{\partial x} \frac{\partial^2}{\partial x^2} \left(\frac{5\hat{u}_2^{(1)}}{108} + \frac{\hat{u}_1^{(1)}}{27} + \frac{2u^{(1)}}{27} \right) \\
&\qquad - d^2 \frac{\partial \hat{u}_1^{(1)}}{\partial x} \frac{\partial^2}{\partial x^2} \left(\frac{\hat{u}_2^{(1)}}{108} - \frac{\hat{u}_1^{(1)}}{27} + \frac{53u^{(1)}}{216} \right) + d^2 \frac{\partial \hat{u}_2^{(1)}}{\partial x} \frac{\partial^2}{\partial x^2} \left(\frac{\hat{u}_2^{(1)}}{108} + \frac{5\hat{u}_1^{(1)}}{108} - \frac{29u^{(1)}}{108} \right).
\end{aligned}
\tag{4.9}
$$

The structure of the forcing terms in the momentum equations (4.7)–(4.9) remains the same as in (4.2), but the terms are expanded to include contributions from the velocity variations $\hat{u}_1$ and $\hat{u}_2$. All three systems contain the same continuity equation, meaning that the vertical flow structure associated with the non-hydrostatic pressure influences the nonlinearity through the momentum equations only.

Investigation of dispersion and nonlinearity for the Boussinesq equations has been on-going for decades. Nwogu (1993) improved the linear dispersion relation of Peregrine (1967) from a [0, 2] to a [2, 2] Padé approximation, while retaining terms consistent with a weakly nonlinear assumption. The second-order governing equations read

$$
\frac{\partial \zeta^{(2)}}{\partial t} + d \frac{\partial u^{(2)}}{\partial x} + (\alpha + \tfrac{1}{3}) d^3 \frac{\partial^3 u^{(2)}}{\partial x^3} = -\zeta^{(1)} \frac{\partial u^{(1)}}{\partial x} - u^{(1)} \frac{\partial \zeta^{(1)}}{\partial x},
\tag{4.10}
$$

$$\frac{\partial u^{(2)}}{\partial t}+g\frac{\partial \zeta^{(2)}}{\partial x}+\alpha d^2\frac{\partial^3 u^{(2)}}{\partial x^2\,\partial t}=-u^{(1)}\frac{\partial u^{(1)}}{\partial x}, \tag{4.11}$$

in which the forcing consists of first-order derivatives derived from the free-surface boundary condition and the advection terms not associated with dispersion. The free parameter α modulates the dispersion properties through the homogeneous part of the second-order governing equations. When $\alpha=-1/3$, the governing equations reduce to those of the classical Boussinesq formulation of Peregrine (1967) and share the same basic structure as the one-layer system. Wei *et al.* (1995) continued using the free parameter to maintain second-order accuracy in dispersion, but developed a set of fully nonlinear governing equations. At second-order, the governing equations are

$$\begin{aligned}&\frac{\partial \zeta^{(2)}}{\partial t}+d\frac{\partial u^{(2)}}{\partial x}+(\alpha+\tfrac{1}{3})d^3\frac{\partial^3 u^{(2)}}{\partial x^3}\\&\quad=-\zeta^{(1)}\frac{\partial u^{(1)}}{\partial x}-u^{(1)}\frac{\partial \zeta^{(1)}}{\partial x}-\alpha d^2\zeta^{(1)}\frac{\partial^3 u^{(1)}}{\partial x^3}-\alpha d^2\frac{\partial \zeta^{(1)}}{\partial x}\frac{\partial^2 u^{(1)}}{\partial x^2},\end{aligned} \tag{4.12}$$

$$\begin{aligned}\frac{\partial u^{(2)}}{\partial t}+g\frac{\partial \zeta^{(2)}}{\partial x}+\alpha d^2\frac{\partial^3 u^{(2)}}{\partial x^3}&=-u^{(1)}\frac{\partial u^{(1)}}{\partial x}+d\frac{\partial \zeta^{(1)}}{\partial x}\frac{\partial^2 u^{(1)}}{\partial x\,\partial t}+d\zeta^{(1)}\frac{\partial^3 u^{(1)}}{\partial x^2\,\partial t}\\&\quad-(\alpha+1)d^2\frac{\partial u^{(1)}}{\partial x}\frac{\partial^2 u^{(1)}}{\partial x^2}-\alpha d^2u^{(1)}\frac{\partial^3 u^{(1)}}{\partial x^3}.\end{aligned} \tag{4.13}$$

The homogeneous part of the governing equations remains the same as Nwogu (1993) owing to the same formulation for dispersion. However, the fully nonlinear formulation introduces additional forcing terms at third degree due to coupling between dispersion and nonlinearity. The presence of α in the forcing terms of the continuity and momentum equations demonstrates the influence of dispersion on nonlinearity even at second order. The momentum equation (4.13) contains five of the six forcing terms in the multi-layer formulation except for the surface curvature term $(\partial^2\zeta/\partial x^2)(\partial u/\partial t)$.

Gobbi *et al.* (2000) extended the approximation of the dispersion relation to the fourth order of kd while retaining full nonlinearity in the resulting Boussinesq equations. Since the original formulation is based on a velocity potential, we rederive the governing equations in terms of the velocity for direct comparison. At second order, the governing equations read

$$\begin{aligned}&\frac{\partial \zeta^{(2)}}{\partial t}+d\frac{\partial u^{(2)}}{\partial x}+\frac{d^3}{2}\left(B-\frac{1}{3}\right)\frac{\partial^3 u^{(2)}}{\partial x^3}+\frac{d^5}{4}\left(B^2-\frac{B}{3}-\frac{D}{6}+\frac{1}{30}\right)\frac{\partial^5 u^{(2)}}{\partial x^5}\\&\quad=-\zeta^{(1)}\frac{\partial u^{(1)}}{\partial x}-u^{(1)}\frac{\partial \zeta^{(1)}}{\partial x}+d^2\left(\frac{1}{2}-\frac{B}{2}\right)\left(\frac{\partial \zeta^{(1)}}{\partial x}\frac{\partial^2 u^{(1)}}{\partial x^2}+\zeta^{(1)}\frac{\partial^3 u^{(1)}}{\partial x^3}\right)\\&\qquad+d^4\left(\frac{D}{24}-\frac{1}{24}-\frac{B^2}{4}+\frac{B}{4}\right)\left(\frac{\partial \zeta^{(1)}}{\partial x}\frac{\partial^4 u^{(1)}}{\partial x^4}+\zeta^{(1)}\frac{\partial^5 u^{(1)}}{\partial x^5}\right),\\&\frac{\partial u^{(2)}}{\partial t}+g\frac{\partial \zeta^{(2)}}{\partial x}+\frac{d^2}{2}(B-1)\frac{\partial^3 u^{(2)}}{\partial x^2\,\partial t}+\frac{d^4}{4}\left(B^2-B-\frac{D}{6}+\frac{1}{6}\right)\frac{\partial^5 u^{(2)}}{\partial x^4\,\partial t}\\&\quad=-u^{(1)}\frac{\partial u^{(1)}}{\partial x}+d\frac{\partial \zeta^{(1)}}{\partial x}\frac{\partial^2 u^{(1)}}{\partial x\,\partial t}+d\zeta^{(1)}\frac{\partial^3 u^{(1)}}{\partial x^2\,\partial t}+d^2\left(-\frac{B}{2}+\frac{1}{2}\right)u^{(1)}\frac{\partial^3 u^{(1)}}{\partial x^3}\end{aligned} \tag{4.14}$$

$$+d^2\left(-\frac{1}{2}-\frac{B}{2}\right)\frac{\partial^2 u^{(1)}}{\partial x^2}\frac{\partial u^{(1)}}{\partial x}+d^3\left(-\frac{1}{6}+\frac{B}{2}\right)\frac{\partial \zeta^{(1)}}{\partial x}\frac{\partial^4 u^{(1)}}{\partial x^3\,\partial t}$$
$$+d^3\left(-\frac{1}{6}+\frac{B}{2}\right)\zeta^{(1)}\frac{\partial^5 u^{(1)}}{\partial x^4\,\partial t}+d^4\left(\frac{B}{4}-\frac{1}{24}-\frac{B^2}{4}+\frac{D}{24}\right)u^{(1)}\frac{\partial^5 u^{(1)}}{\partial x^5}$$
$$+d^4\left(\frac{D}{24}+\frac{1}{8}-\frac{B^2}{4}-\frac{B}{4}\right)\frac{\partial^4 u^{(1)}}{\partial x^4}\frac{\partial u^{(1)}}{\partial x}-d^4\left(\frac{B^2}{4}+\frac{1}{12}\right)\frac{\partial^3 u^{(1)}}{\partial x^3}\frac{\partial^2 u^{(1)}}{\partial x^2}. \quad (4.15)$$

The forcing terms contain fifth-order derivatives of the velocity to further strengthen nonlinear interactions. Similar to Wei *et al.* (1995), the two free parameters alter dispersion in the homogeneous part as well as the strength of the nonlinear forcing. Comparison of the two systems derived from the fully nonlinear Boussinesq equations shows that the second- and fourth-order approximations in dispersion result in third- and fifth-order derivatives in the forcing, signifying the coupling between dispersion and nonlinearity. The highest order of surface elevation derivatives remains at one in the Boussinesq approach. The forcing terms from a low-order approximation of dispersion, such as Wei *et al.* (1995), serves as a subset to a high-order approximation, which is illustrated through the governing equations (4.14) and (4.15) derived from Gobbi *et al.* (2000). In comparison, the governing equations from the multi-layer formulation maintain a degree of three regardless of the number of layers, but involve a second-order derivative to account for the curvature of the free surface.

4.2. *Second-order interactions of monochromatic waves*

The second-order solution, which reflects the leading-order nonlinear interactions, provides a standard for model assessment. The pertinent nonlinear forcing depends on the vertical flow structure resolved by the multi-layer system. Computation of the second-order harmonics due to interactions of first-order waves allows evaluation of model performance in relation to the Boussinesq approach. We consider wave propagation over water of constant depth for derivation of analytical solutions. The first-order monochromatic waves in the multi-layer system can be represented as

$$\zeta^{(1)}(x,t)=a_1\cos(kx-\omega t), \quad (4.16)$$
$$u^{(1)}(x,t)=b_1\cos(kx-\omega t), \quad (4.17)$$
$$\hat{u}_i^{(1)}(x,t)=f_i\cos(kx-\omega t), \quad (4.18)$$

where a_1, b_1 and f_i are the amplitude of the surface elevation, the depth-averaged velocity and applicable velocity variations across interfaces. The linear waves produce self-interacting second-order harmonics in the form

$$\zeta^{(2)}(x,t)=a_2\cos(2kx-2\omega t), \quad (4.19)$$
$$u^{(2)}(x,t)=b_2\cos(2kx-2\omega t), \quad (4.20)$$
$$\hat{u}_i^{(2)}(x,t)=g_i\cos(2kx-2\omega t), \quad (4.21)$$

where a_2, b_2 and g_i vary with the water depth parameter kd. The second-order Stokes wave theory gives the wave amplitude

$$a_{2s}=\tfrac{1}{4}a_1^2k[3\coth^3(kd)-\coth(kd)], \quad (4.22)$$

which is used as a reference for comparison among the solutions obtained from the multi-layer and Boussinesq systems.

Substitution of the first-order harmonics (4.16)–(4.18) into the linearized governing equations of the multi-layer system gives the expressions of b_1 and f_i in terms of a_1. The linear dispersion relation provides an expression for the angular frequency ω in terms of kd. These three expressions consolidate the variables of the first-order harmonics into a_1 and kd as in Airy wave theory. Substitution of the first-order harmonics and the second-order harmonics (4.19)–(4.21) into the second-order governing equations provides a system of algebraic equations from which the solution can be obtained. The second-order governing equations (4.1) and (4.2) of the one-layer system give the wave amplitude as

$$a_{2,1} = \frac{1}{4}a_1^2 k \frac{4 + k^2 d^2}{k^3 d^3}. \tag{4.23}$$

The expression shares a common coefficient with the Stokes solution and utilizes a rational function to approximate the variation of the amplitude with kd. Similarly, the second-order governing equations (4.3)–(4.5) of the two-layer system with the interface at mid-flow depth give

$$a_{2,2} = \frac{1}{4}a_1^2 k \frac{49\,152 + 33\,792k^2d^2 + 9280k^4d^4 + 796k^6d^6 + 15k^8d^8}{3k^3d^3(5120 + 640k^2d^2 + 36k^4d^4 + k^6d^6)}. \tag{4.24}$$

The second-order governing equations (4.6)–(4.9) for three layers with equal thickness give

$$\begin{aligned} a_{2,3} = \frac{a_1^2 k}{4k^3d^3}\Bigg(&\frac{108}{35} + \frac{19}{7}k^2d^2 + \frac{1877}{1890}k^4d^4 + \frac{4741}{29\,160}k^6d^6 + \frac{49\,477}{4898\,880}k^8d^8 \\ &+ \frac{36\,433}{176\,359\,680}k^{10}d^{10} + \frac{4219}{2380\,855\,680}k^{12}d^{12} + \frac{89}{14\,285\,134\,080}k^{14}d^{14}\Bigg) \\ &\times \Bigg(1 + \frac{7}{27}k^2d^2 + \frac{29}{1080}k^4d^4 + \frac{101}{81\,648}k^6d^6 + \frac{3593}{176\,359\,680}k^8d^8 \\ &+ \frac{1}{5878\,656}k^{10}d^{10} + \frac{1}{1587\,237\,120}k^{12}d^{12}\Bigg)^{-1}. \end{aligned} \tag{4.25}$$

All three solutions share a common term k^3d^3 in the denominator. The polynomial in the numerator is two orders higher than that in the denominator. Each additional layer increases the order in the numerator and denominator by six to give a $[6(N-1)+2, 6(N-1)]$ expansion of the Stokes second-order solution.

A similar procedure using the first- and second-order harmonics defined by (4.16), (4.17), (4.19) and (4.20) in the second-order Boussinesq equations provides analytical solutions for comparison. The second-order governing equations (4.10) and (4.11) of Nwogu (1993) give the wave amplitude as

$$a_{2N} = \frac{1}{4}a_1^2 k \frac{9 - 42\alpha k^2d^2 - 6k^2d^2 + 24\alpha^2k^4d^4 + 8\alpha k^4d^4}{k^3d^3(3 - 3\alpha k^2d^2 - k^2d^2)}. \tag{4.26}$$

The expression shares the same coefficient as the Stokes and multi-layer solutions and also utilizes a rational function to approximate the variation of the second-order wave amplitude with kd. An $\alpha = -1/3$ reduces the power in the numerator and denominator by two and gives rise to the second-order solution of the classical Boussinesq equations of Peregrine (1967) with the same structure as the one-layer solution (4.23). The second-order governing equations (4.12) and (4.13) of Wei *et al.*

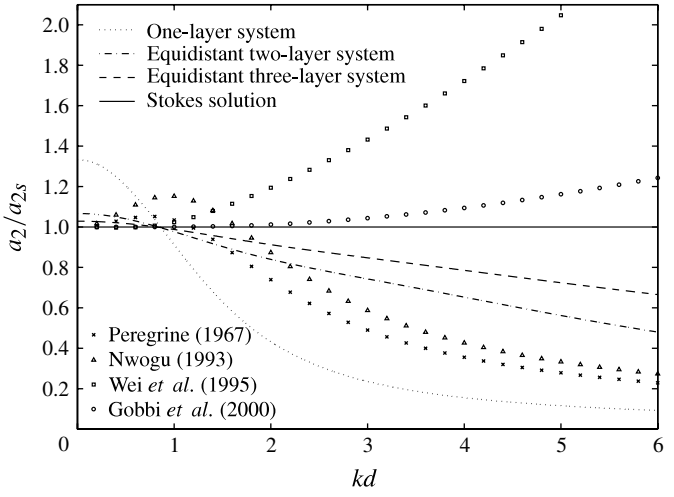

FIGURE 5. Normalized amplitude of self-interacting super-harmonics from multi-layer and Boussinesq models.

(1995) give

$$a_{2W} = \frac{a_1^2 k}{12k^3d^3}[-27 + (45 + 162\alpha)k^2d^2 + (-42 - 180\alpha - 234\alpha^2)k^4d^4 + (8 + 48\alpha + 96\alpha^2 + 72\alpha^3)k^6d^6][-3 + (3\alpha + 1)k^2d^2]^{-1}. \tag{4.27}$$

The power of the polynomial in the denominator remains the same as the solution (4.26) from Nwogu (1993) because of the same [2, 2] Padé approximation of dispersion. However, the fully nonlinear formulation of Wei *et al.* (1995) raises the power in the numerator by two. The second-order governing equations (4.14) and (4.15) of Gobbi *et al.* (2000) with the optimal free parameters, $B = 1/9$ and $D = 5/189$, give

$$a_{2G} = \frac{a_1^2 k}{24k^3d^3}\left(64\,800 + 64\,800k^2d^2 + \frac{190\,080}{7}k^4d^4 + \frac{361\,280}{63}k^6d^6 + \frac{30\,080}{63}k^8d^8 + \frac{18\,176}{1323}k^{10}d^{10} + \frac{8192}{83\,349}k^{12}d^{12}\right)\left(3600 + 1200k^2d^2 + \frac{1040}{7}k^4d^4 + \frac{4000}{567}k^6d^6 + \frac{704}{11\,907}k^8d^8\right)^{-1}. \tag{4.28}$$

The [4, 4] Padé approximation of dispersion increases the power in the numerator and denominator by six analogous to an additional layer in the multi-layer formulation. While the Boussinesq solutions share the same coefficient $a_1^2k/4$ and the common term k^3d^3 as in the multi-layer models, their convergence follows a $[6L, 6M - 4]$ expansion corresponding to the highest odd-order derivative of $(2L + 1)$ and $(2M + 1)$ in the first-order continuity and momentum equations.

The structure of the solution is a manifestation of the flow field approximation in the vertical direction and its effects on nonlinearity in the multi-layer and Boussinesq approaches. Figure 5 compares the second-order wave amplitudes obtained from the two approaches. The results are normalized with the Stokes solution (4.22) and thus

unity indicates perfect agreement. The four Boussinesq solutions converge to the Stokes solution as kd approaches zero and dispersion becomes negligible. Since the high-order nonlinear terms diminish along with dispersion, all four Boussinesq formulations give the same second-order governing equations at the shallow-water limit. As kd increases, the solutions from Peregrine (1967) and Nwogu (1993) show distinct convergence characteristics due to the weakly nonlinear assumptions in comparison to the fully nonlinear approach of Wei *et al.* (1995) and Gobbi *et al.* (2000). The Boussinesq approach describes the vertical flow structure through Taylor series expansions. Even with the fully nonlinear formulation, the increase from a [2, 2] to a [4, 4] Padé approximation of the dispersion also improves the nonlinear solution. The multi-layer approach exhibits a different pattern of convergence. The solution shows an offset towards $kd = 0$ that is not seen in the Boussinesq models. This might be due to the slower convergence of the dispersion relation in shallow water associated with the local peak of relative errors as seen in figure 3. The errors in the second-order amplitude decrease to zero around $kd = 0.8$ and then the solutions diverge with larger values of kd. The multi-layer approach resolves the vertical flow structure through a piecewise linear approximation, which in the present equidistant layer arrangement requires a considerable number of layers to provide satisfactory descriptions of the nonlinear advection terms and free-surface boundary condition.

An alternative approach to improve the nonlinear properties of a multi-layer model is to reduce the layer thickness towards the free surface. This provides a more accurate description of the surface velocity for the free-surface boundary condition (2.21). For the two-layer model, adjustment of the interface from mid-flow depth may compromise the dispersion properties as shown in figure 2. To overcome this problem, we introduce a predefined piecewise linear distribution of the non-hydrostatic pressure involving a free parameter α, which can be adjusted to achieve desirable wave properties (Bai & Cheung 2013). The second-order governing equations maintain the same structure as the two-layer system (4.3)–(4.5), but with different coefficients in the momentum equations. The second-order wave amplitude becomes

$$\hat{a}_{2,2} = \frac{a_1^2 k}{96k^3d^3}[3072 + (1536 + 768\alpha)k^2d^2 + (420 + 432\alpha - 256\alpha^2)k^4d^4 + (27 + 24\alpha - 16\alpha^2)k^6d^6][(1 + 2\alpha)(16 + k^2d^2)]^{-1}. \tag{4.29}$$

The solution has the same structure as (4.27) from the second-order formulation of Wei *et al.* (1995). The three-layer system has two free parameters r_1 and r_2 for adjustment of the layer structure to optimize the nonlinear properties. In the optimization, we minimize the error function

$$\text{error} = \int_{0.01}^{\sigma} \left| \frac{\hat{a}_2}{a_{2s}} - 1 \right| \mathrm{d}(kd), \tag{4.30}$$

where σ is the upper limit of the integration appropriate to the applicable range of the model.

Figure 6 shows the computed error distributions for the two- and three-layer systems as functions of the respective free parameters. The error of the two-layer model is computed for kd up to 3 because of the applicable range of dispersion associated with the predefined pressure distribution (Bai & Cheung 2013). An $\alpha \approx 0.85$ gives the minimum error of 0.054 in the second-order wave amplitude as well as a [2, 2] Padé approximation for optimization of the dispersion properties to the same level as Nwogu (1993) and Wei *et al.* (1995). For the three-layer system, we integrate the

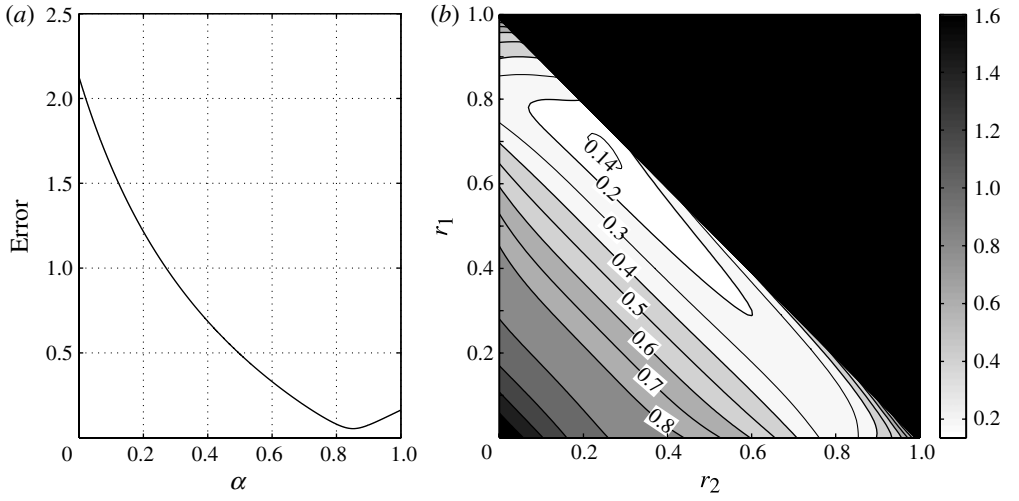

FIGURE 6. Relative errors for the (*a*) two-layer and (*b*) three-layer systems as functions of free parameters.

error up to $kd = 6$ for the wider applicable range of the model. The results show a combination of $r_1 = 0.68$ and $r_2 = 0.25$ yields the minimum relative error of 0.1357. In this layer arrangement, the bottom layer extends above mid-flow depth and a thin top layer with $r_3 = 0.07$ provides a close approximation of the surface velocity for the free-surface boundary condition. In terms of dispersion, this gives a low relative error of 0.038 versus the optimal value of 0.031 from (3.29) based on three equidistant layers. Application of this arrangement gives the second-order wave amplitude for the three-layer system as

$$\begin{aligned}\hat{a}_{2,3} = \frac{a_1^2 k}{4k^3 d^3}&(1.024\,000\,001 \times 10^{26} + 6.925\,311\,982 \times 10^{25} k^2 d^2 \\ &+ 2.087\,888\,438 \times 10^{25} k^4 d^4 + 2.662\,461\,251 \times 10^{24} k^6 d^6 \\ &+ 9.274\,286\,497 \times 10^{22} k^8 d^8 + 9.474\,052\,981 \times 10^{20} k^{10} d^{10} \\ &+ 4.245\,247\,576 \times 10^{18} k^{12} d^{12} + 4.009\,016\,022 \times 10^{15} k^{14} d^{14}) \\ &\times (3.131\,392\,000 \times 10^{25} + 4.374\,412\,800 \times 10^{24} k^2 d^2 + 2.596\,243\,523 \times 10^{23} k^4 d^4 \\ &+ 7.093\,462\,058 \times 10^{21} k^6 d^6 + 3.599\,832\,971 \times 10^{19} k^8 d^8 \\ &+ 8.807\,100\,983 \times 10^{16} k^{10} d^{10} + 1.108\,391\,289 \times 10^{14} k^{12} d^{12})^{-1}. \end{aligned} \tag{4.31}$$

The expression maintains the same structure as (4.25) for three equidistant layers, but with different coefficients to account for the optimal layer arrangement.

Figure 7 compares the second-order wave amplitudes from the fully nonlinear Boussinesq formulations and the optimized two- and three-layer models. For the Boussinesq formulations, the amplitude relative to the Stokes solution is equal to one at the shallow-water limit and increases monotonically with kd. The solutions from Wei *et al.* (1995) and Gobbi *et al.* (2000) begin to deviate from the Stokes solution by 10 % at $kd = 1.52$ and 4.1 and lead to overestimations of 139.3 and 24.3 % at $kd = 6$. The optimized two-layer system shows similar convergence characteristics as the Boussinesq approach and represents a major improvement on the original two-layer model due to improvement of the dispersion properties in shallow and intermediate

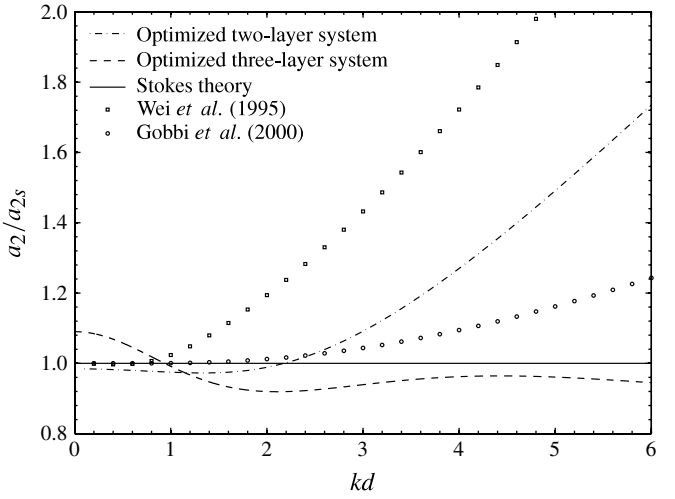

FIGURE 7. Normalized amplitude of self-interacting super-harmonics from optimized multi-layer and Boussinesq models.

water. It has a relative amplitude of 0.9844 at $kd = 0$. The value drops slightly to 0.9726 around $kd = 1.3$ and maintains a maximum of 1.044 within its applicable range of $kd \leqslant 3$. The three-layer system gives a relative amplitude of 1.09 at $kd = 0$, shows a downward trend, reaching a minimum of 0.92 at $kd = 2$, and then varies between 0.94 and 0.96 from $kd = 3$ to 6. In general, the Boussinesq formulations yield close approximations of the Stokes solution in shallow and intermediate water, but overestimate the second-order wave amplitude due to stronger nonlinear forcing in deep water. The optimized two-layer system provides reasonable approximations in the range of $kd \leqslant 3$ for coastal wave transformation. The three-layer system maintains an error of less than 10 % and provides a reliable approximation of the second-order wave amplitude over the range of kd considered here.

4.3. *Second-order interactions of bichromatic waves*

Nonlinear surface waves interact with each other to generate super-harmonics at the sum of the frequencies and sub-harmonics at the difference of the frequencies by which energy is transferred from the peak to the sidebands of the spectrum. The second-order interactions between two first-order wave components play a fundamental role in this process and provide a metric for assessment of model capabilities in reproducing nonlinear properties. For a multi-layer system, a first-order wave group consisting of two wave frequencies ω_m and ω_n with the corresponding wavenumbers k_m and k_n can be written as

$$\zeta^{(1)}(x, t) = a_m \cos(k_m x - \omega_m t) + a_n \cos(k_n x - \omega_n t), \tag{4.32}$$

$$u^{(1)}(x, t) = \frac{\omega_m}{k'_{um} d} a_m \cos(k_m x - \omega_m t) + \frac{\omega_n}{k'_{un} d} a_n \cos(k_n x - \omega_n t), \tag{4.33}$$

$$\hat{u}_i^{(1)}(x, t) = \frac{\omega_m}{k'_{\hat{u}_i m} d} a_m \cos(k_m x - \omega_m t) + \frac{\omega_n}{k'_{\hat{u}_i n} d} a_n \cos(k_n x - \omega_n t), \tag{4.34}$$

where a_m and a_n are wave amplitudes and the coefficients k'_{um}, k'_{un}, $k'_{\hat{u}_i m}$ and $k'_{\hat{u}_i n}$ are determined from the respective first-order governing equations. Let $\theta_m = k_m x - \omega_m t$

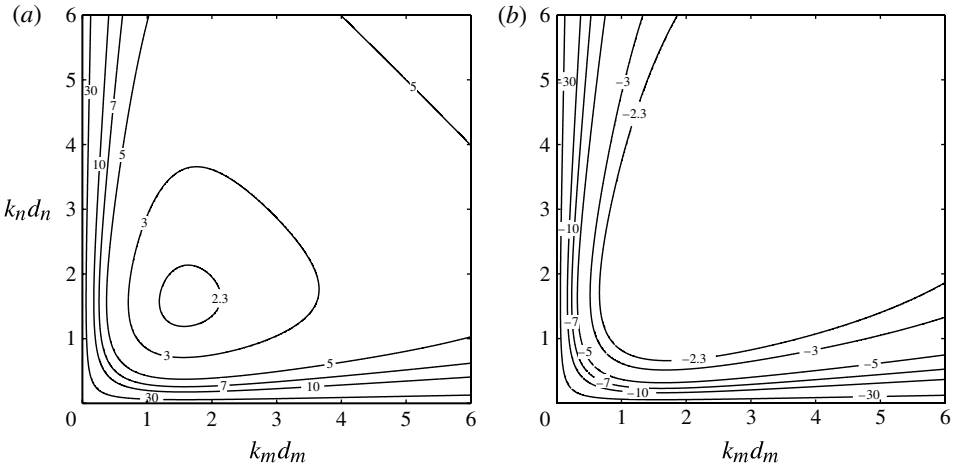

FIGURE 8. Amplitude of (*a*) super-harmonics and (*b*) sub-harmonics from second-order Stokes theory.

and $\theta_n = k_n x - \omega_n t$ for abbreviation of the second-order solutions. Self- and cross-interactions of the bichromatic waves defined by (4.32)–(4.34) force the development of four second-order components, which include three super-harmonics at $2\theta_m$, $2\theta_n$ and $(\theta_m + \theta_n)$ and one sub-harmonic at $(\theta_m - \theta_n)$. The resulting second-order solution can be written in the form

$$\zeta^{(2)}(x,t) = a_m a_n G_\zeta^{m+n} \cos(\theta_m + \theta_n) + \tfrac{1}{2} a_m^2 G_\zeta^{2m} \cos(2\theta_m) + a_m a_n H_\zeta^{m-n} \cos(\theta_m - \theta_n) + \tfrac{1}{2} a_n^2 G_\zeta^{2n} \cos(2\theta_n), \tag{4.35}$$

$$u^{(2)}(x,t) = a_m a_n G_u^{m+n} \cos(\theta_m + \theta_n) + \tfrac{1}{2} a_m^2 G_u^{2m} \cos(2\theta_m) + a_m a_n H_u^{m-n} \cos(\theta_m - \theta_n) + \tfrac{1}{2} a_n^2 G_u^{2n} \cos(2\theta_n), \tag{4.36}$$

$$\hat{u}_i^{(2)}(x,t) = a_m a_n G_{\hat{u}_i}^{m+n} \cos(\theta_m + \theta_n) + \tfrac{1}{2} a_m^2 G_{\hat{u}_i}^{2m} \cos(2\theta_m) + a_m a_n H_{\hat{u}_i}^{m-n} \cos(\theta_m - \theta_n) + \tfrac{1}{2} a_n^2 G_{\hat{u}_i}^{2n} \cos(2\theta_n), \tag{4.37}$$

where G and H are the super- and sub-harmonic transfer functions for the subscripted flow variables and superscripted wave components. Substitution of the first- and second-order bichromatic groups from (4.32)–(4.34) and (4.35)–(4.37) into the second-order governing equations of the two- and three-layer systems yields sets of algebraic equations from which the quadratic transfer functions can be evaluated.

The transfer function of the self-interacting super-harmonics $2\theta_m$ and $2\theta_n$ has been derived and examined in § 4.2. The transfer functions of the cross-interacting super-harmonics $(\theta_m + \theta_n)$ and sub-harmonics $(\theta_m - \theta_n)$ are investigated here. Published transfer functions of the super- and sub-harmonics have been derived as functions of $\omega\sqrt{d/(4\pi^2 g)}$ from the second-order free-surface boundary conditions of Stokes wave theory (Ottesen-Hansen 1978; Dean & Sharma 1981; Sand & Mansard 1986). We express their transfer functions in terms of kd as shown in figure 8 to provide a basis for comparison. Since $k_m d$ and $k_n d$ are interchangeable, both contour plots are symmetric about the diagonal $k_m d = k_n d$, which corresponds to the self-interacting components. The super-harmonics modify the first-order wave profile by elevating the crest and flattening the trough. The transfer function has a minimum in the range of

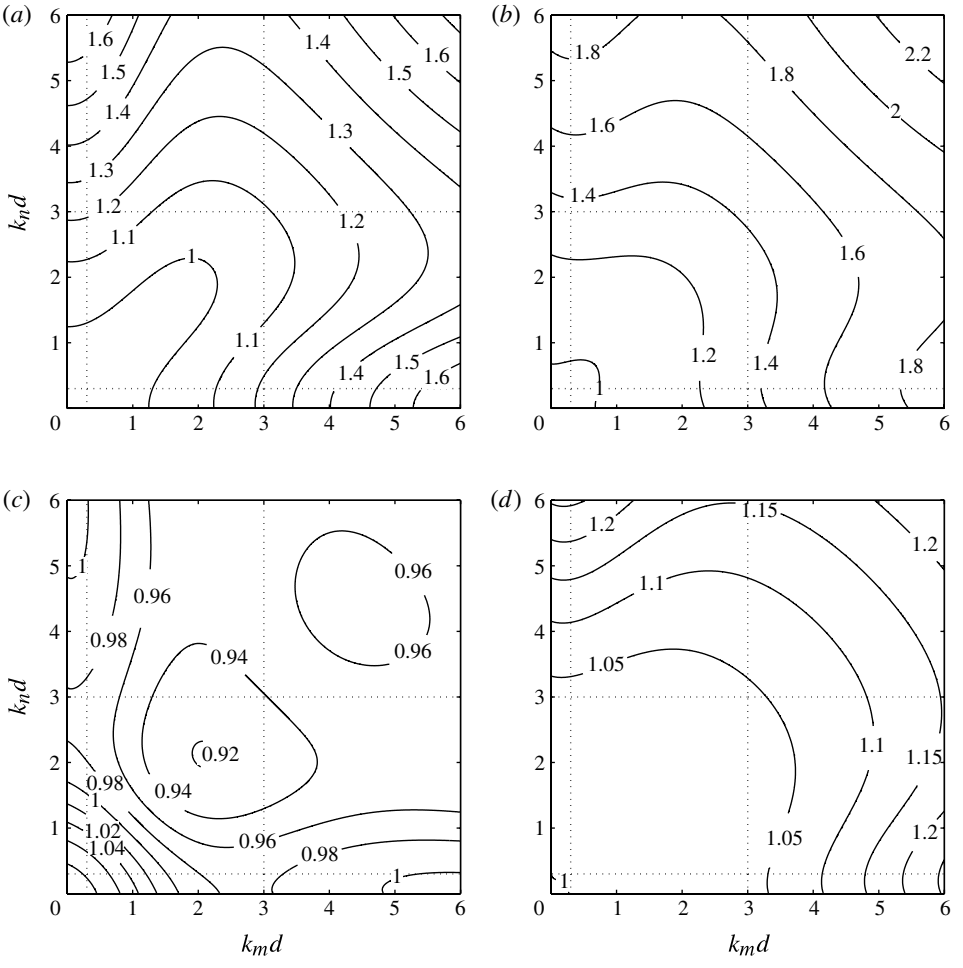

FIGURE 9. Normalized amplitude of super-harmonics from optimized multi-layer and Boussinesq models: (*a*) optimized two-layer system; (*b*) Wei *et al.* (1995); (*c*) optimized three-layer system; (*d*) Gobbi *et al.* (2000).

intermediate waves and increases for longer and shorter waves. The sub-harmonics are bounded long waves that modulate the surface elevation along a wave group. The absolute value of the transfer function increases from short to long waves and converges to the setdown when k_md approaches k_nd. These low-frequency waves are closely related to many coastal phenomena such as harbour resonance, surf beats and coastal sediment transport.

Figure 9 plots the transfer functions of the super-harmonics from the optimized two- and three-layer models and the fully nonlinear Boussinesq models. The results are normalized by the second-order Stokes solution, and each panel shows contour lines of the relative amplitude at equal intervals. Based on the upper limit of long waves at $kd = 0.3$ and the lower limit of short waves at $kd = 3$, the two-dimensional plots in terms of kd are divided into nine segments for discussion. The diagonal segments correspond to interactions between two long-, two intermediate- and two short-wave components at first order and the relative amplitude follows closely with

the results of self-interacting second harmonics in figure 7. In the segment for long-wave interactions, the Boussinesq and two-layer models produce nearly the same transfer function as the Stokes wave theory, whereas the three-layer model gives slightly higher relative amplitude of 1.07–1.09. The capability to describe nonlinear interactions of intermediate waves varies among the four models. The formulation of Wei *et al.* (1995) shows considerable errors, with the relative amplitude ranging from 0.9967 to 1.4323, while the formulation of Gobbi *et al.* (2000) has a smaller range from 1 to 1.0436. The two-layer model performs better than Wei *et al.* (1995), with a relative amplitude range of 0.9726–1.2152. The three-layer model gives a relative amplitude of 1.0777 towards the long-wave limit, but with a value as low as 0.9192 at the short-wave limit. It is desirable to have a coastal wave transformation model that can describe deep-water input wave conditions at $kd \geqslant 3$. The Boussinesq model of Wei *et al.* (1995), which overestimates the super-harmonics with relative amplitude of 1.4323 at $kd = 3$, might not properly describe the nonlinearity of the input wave conditions at deep water. The two-layer model and the Boussinesq formulation of Gobbi *et al.* (2000) slightly overestimate the super-harmonics with relative amplitude of 1.0913 and 1.0436, while the three-layer model provides a slight underestimation of 0.9392 towards this limit. In the segment of short-wave interaction, the three-layer system and the Boussinesq model of Gobbi *et al.* (2000) yield reasonable results, with a slight underestimation of 0.9392–0.9642 and an overestimation from 1.0436 to 1.2431, respectively. The two-layer system and the Boussinesq model of Wei *et al.* (1995) are not applicable in this range because of the limited capability in dispersion that adversely influences the model nonlinearity.

The transfer functions in figure 9 also illustrate the model capability to account for second-order interactions between long and intermediate waves, long and short waves, and intermediate and short waves. In particular, nonlinear interactions between long and intermediate waves become important when surf beat develops from wave breaking in the surf zone. The Boussinesq model of Wei *et al.* (1995) has the largest range of relative amplitude from 0.9972 to 1.3560 among the four models. The two-layer model presents a range of relative amplitude from 0.9824 to 1.2227. Both the three-layer model and the Boussinesq model of Gobbi *et al.* (2000) provide close approximations over this segment, with relative amplitude ranging from 0.9740 to 1.0855 and 1 to 1.0363, respectively. Overall, both the two- and three-layer models have favourable nonlinear properties to describe the super-harmonics for wave transformation from deep to shallow water. They have relatively low errors over a wide band along the diagonal extending to the upper limit of the intermediate waves. This is important for definition of the input deep-water wave conditions and steepening of wave profiles prior to wave breaking. They also produce low errors for cross-interactions between long and immediate waves in the surf zone. In addition, the three-layer model yields reasonable results even in the short-wave interaction segment.

Sub-harmonic interactions are equally important in the coastal processes related to infragravity waves and resonance. Figure 10 plots the normalized transfer functions from the two multi-layer models and the two Boussinesq models. For long-wave interactions, the Boussinesq and two-layer models produce very good agreement with the second-order Stokes solution. The three-layer model gives slightly higher relative amplitude of 1.09 as in the case of the super-harmonics. In the intermediate range, the relative amplitude from the Boussinesq models decreases to a negative value at the short-wave limit near the diagonal. The solutions deteriorate rapidly and the amplitudes become mostly negative in the short-wave segment. The negative sign denotes a 180° phase shift of the sub-harmonics with respect to the Stokes solution.

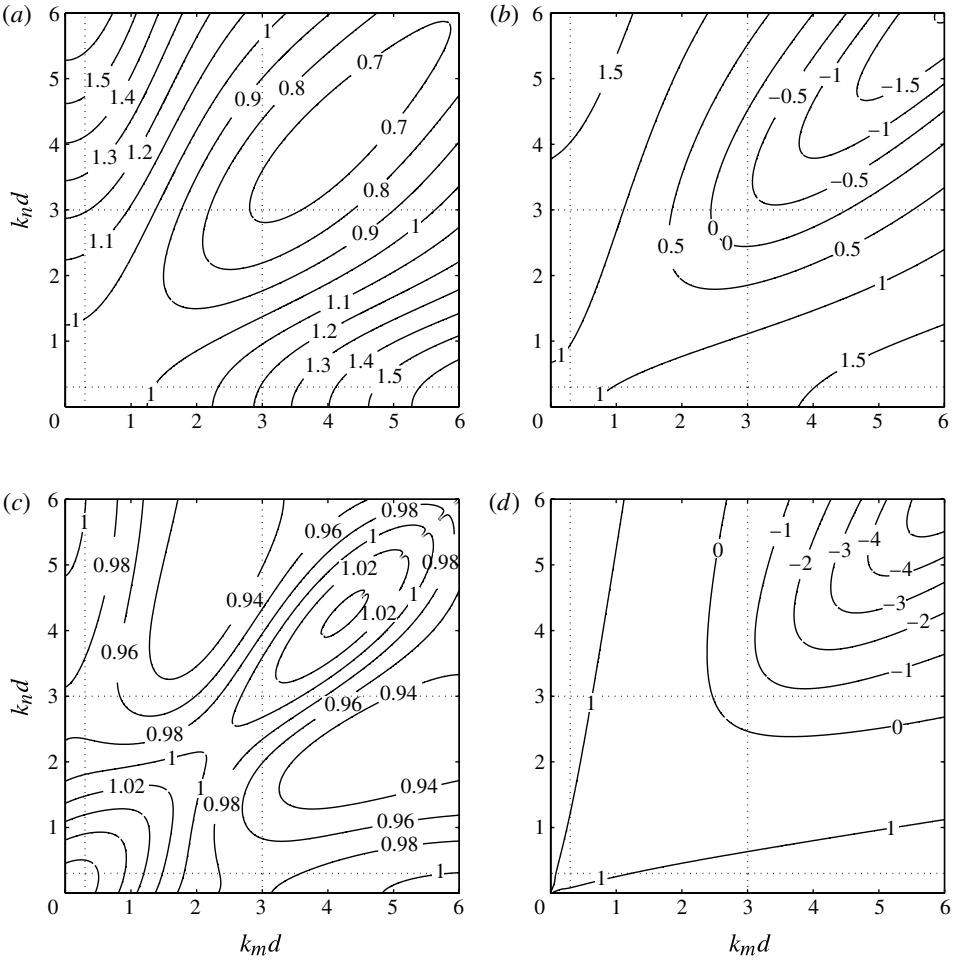

FIGURE 10. Normalized amplitude of sub-harmonics from optimized multi-layer and Boussinesq models: (*a*) optimized two-layer system; (*b*) Wei *et al.* (1995); (*c*) optimized three-layer system; (*d*) Gobbi *et al.* (2000).

The two-layer model also shows a decreasing trend, but remains positive throughout the intermediate- and short-wave segments. It gives a relative amplitude as low as 0.6427 along the diagonal and up to 1.2061 in the off-diagonal directions. Only the three-layer system is able to produce accurate approximations in the short-wave segment, with relative amplitude ranging from 0.9153 to 1.043. Cross-interactions between short and long waves are not important for generation of sub-harmonics because of the large difference in frequency. Nevertheless, the two-layer model can reasonably approximate the sub-harmonic interactions between long and intermediate waves, and the three-layer system can describe the interactions between intermediate and short waves as well.

The sub-harmonics convert to steady setdown of the water level at the limiting condition of $k_m d \rightarrow k_n d$. Figure 11 compares the normalized setdown computed from the multi-layer and Boussinesq approaches. The solutions from the Boussinesq models of Wei *et al.* (1995) and Gobbi *et al.* (2000) converge to the Stokes solution in

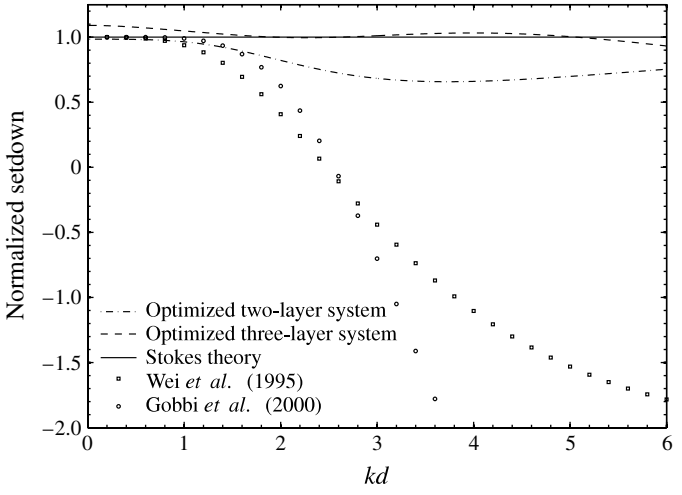

FIGURE 11. Normalized wave setdown from optimized multi-layer and Boussinesq models.

shallow water and gradually deteriorate with increasing kd. The relative errors of the two solutions reach 50 % at $kd = 1.88$ and 2.14, respectively. Instead of predicting wave setdown, both Boussinesq models produce an increase of the water level around $kd > 2.6$ as documented in Gobbi *et al.* (2000). Reproduction of the setdown, or the sub-harmonic wave amplitude in general, with the Boussinesq approach requires a much higher-order expansion of the velocity profile (Madsen *et al.* 2003). The two-layer model closely approximates the Stokes solution for $kd < 1$ and maintains a positive value for the range kd considered. The three-layer model gives the best overall agreement despite having an 8 % offset towards $kd = 0$. A multi-layer model resolves the flow through a piecewise linear distribution and manages to approximate a deep-water velocity profile without creating artificial flow reversals as seen in Boussinesq models with low-order expansions. It should be pointed out the two- and three-layer models are respectively optimized over $0 \leqslant kd \leqslant 3$ and $0 \leqslant kd \leqslant 6$ for comparison with the Boussinesq models of Wei *et al.* (1995) and Gobbi *et al.* (2000). The multi-layer approach has the flexibility to optimize the dispersion and nonlinear properties for specific applications.

5. Conclusions

This study has introduced a new multi-layer formulation for non-hydrostatic free-surface flows and examined its linear and nonlinear wave properties in relation to the Boussinesq approach. Depth integration of the fluid layers results in a piecewise linear distribution of the velocity profile. A linear transformation recasts the conventional multi-layer formulation into a series form with flux- and dispersion-dominated components, which allows modelling of discontinuities through momentum conservation and maintains the same dispersion characteristics. The integrated multi-layer system explicitly describes the vertical flow structure through a depth-averaged velocity and the variations between adjacent layers. Refinement of the velocity profile with additional layers expands the dispersion-dominated system, but does not modify the continuity equation in conserving mass. The direct coupling of the flow at all layers facilitates efficient advection beyond the layer boundaries for transport and redistribution of mass and momentum over the water column.

The proposed governing equations, which define analytically a multi-layer flow, allow conversion into a Boussinesq form with the vertical velocity and non-hydrostatic pressure eliminated. Implementation of a perturbation expansion separates the resulting governing equations into first and second order for optimization of wave properties and direct comparison with the Boussinesq equations. The linearized system utilizes third-order derivatives of the velocity terms to account for dispersion regardless of the number of layers. The dispersion relation for an N-layer system follows a $[2N-2, 2N]$ Padé expansion associated with the piecewise linear distribution of the velocity profile. Numerical results for up to three layers show that the equidistant layer arrangement gives the best agreement with the exact linear dispersion relation. In comparison, the Boussinesq approach utilizes a predefined expansion of the vertical flow structure that results in high-order derivatives of the velocity. This gives rise to a $[2L, 2M]$ Padé approximation of the dispersion relation corresponding to the highest odd-order derivative of $(2L+1)$ and $(2M+1)$ in the continuity and momentum equations. At comparable orders of expansion, the Boussinesq approach gives a slightly better description of wave dispersion in shallow and intermediate water depth. The multi-layer approach can maintain proper dispersion characteristics into deeper water.

The second-order governing equations determine the leading-order nonlinear interactions between wave components. The multi-layer system involves six sets of nonlinear forcing terms in the momentum equations, with a highest degree of three, including one with second-order spatial derivatives of the surface elevation. The second-order wave amplitude is in the form of a rational function, which represents a $[6(N-1)+2, 6(N-1)]$ expansion of the second-order Stokes solution. This expansion produces a small error in shallow water that decreases with increasing number of layers. A predefined piecewise non-hydrostatic pressure profile in an equidistant two-layer model and a thin surface layer in a three-layer model can effectively capture super- and sub-harmonics over a wide range of kd. The fully nonlinear Boussinesq equations results in higher-degree forcing terms that are comparable to five of the forcing terms in the multi-layer approach, but does not include an equivalent surface curvature term. It leads to a $[6L, 6M-4]$ expansion of the exact solution. This expansion gives accurate results towards the shallow-water limit $kd=0$, but falls short of providing a reasonable approximation for the sub-harmonics in deep water, as already reported in the literature. At comparable orders of expansion, the multi-layer approach can provide better approximations of both the super- and sub-harmonics in deep water owing to the more adaptive vertical flow structure.

Acknowledgements

This study was funded by the Office of Naval Research grant number N00014-02-1-0903 and the National Tsunami Hazard Mitigation Program contract number NA08NWS4670033. We would like to thank the associate editor and the two anonymous reviewers for the comments and suggestions that have improved this paper. SOEST Contribution Number 8819.

REFERENCES

AGNON, Y., MADSEN, P. A. & SCHÄFFER, H. A. 1999 A new approach to high order Boussinesq models. *J. Fluid Mech.* **399**, 319–333.

AI, C. & JIN, S. 2012 A multi-layer non-hydrostatic model for wave breaking and runup. *Coast. Engng* **62**, 1–8.

AI, C., JIN, S. & LV, B. 2011 A new fully non-hydrostatic 3D free surface model for water wave motions. *Intl J. Numer. Meth. Fluids* **66**, 1354–1370.

BAI, Y. 2012 Depth-integrated free-surface flow with non-hydrostatic formulation. PhD dissertation, University of Hawaii, Honolulu.

BAI, Y. & CHEUNG, K. F. 2012 Depth-integrated free-surface flow with a two-layer non-hydrosatic formulation. *Intl J. Numer. Meth. Fluids* **69** (2), 411–429.

BAI, Y. & CHEUNG, K. F. 2013 Depth-integrated free-surface flow with parameterized non-hydrostatic pressure. *Intl J. Numer. Meth. Fluids* **71** (4), 403–421.

CASULLI, V. 1995 Recent developments in semi-implicit numerical methods for free surface hydrodynamics. In *Proceedings of the Second International Conference on Hydroscience and Engineering, Beijing*, Advances in Hydro Science and Engineering, vol. 2, Part B, pp. 2174–2181.

CASULLI, V. 1999 A semi-implicit finite difference method for non-hydrostatic, free-surface flows. *Intl J. Numer. Meth. Fluids* **30**, 425–440.

CASULLI, V. & STELLING, G. S. 1998 Numerical simulation of 3D quasi-hydrostatic, free-surface flows. *J. Hydraul. Engng ASCE* **124**, 678–686.

DEAN, R. G. & SHARMA, J. N. 1981 Simulation of wave systems due to nonlinear directional spectra. In *Proceedings of the International Symposium on Hydrodynamics in Ocean Engineering, Norwegian Institute of Technology, Trondheim*, vol. 2, pp. 1211–1222.

GOBBI, M. F., KIRBY, J. T. & WEI, G. 2000 A fully nonlinear Boussinesq model for surface waves. Part 2. Extension to $O(kh)^4$. *J. Fluid Mech.* **405**, 181–210.

KAZOLEA, M., DELIC, A. I., NIKOLOS, I. K. & SYNOLAKIS, C. E. 2012 An unstructured finite volume numerical scheme for extended 2D Boussinesq-type equations. *Coast. Engng* **69**, 42–66.

LAY, T., AMMON, C. J., YAMAZAKI, Y., CHEUNG, K. F. & HUTKO, A. R. 2011 The 25 October 2010 Mentawai tsunami earthquake and the tsunami hazard presented by shallow megathrust ruptures. *Geophys. Res. Lett.* **38**, L06302.

LYNETT, P. J. & LIU, P. L. 2004*a* Linear analysis of the multi-layer model. *Coast. Engng* **51**, 439–454.

LYNETT, P. J. & LIU, P. L. 2004*b* A two-layer approach to wave modelling. *Proc. R. Soc.* A **460**, 2637–2669.

MA, G., SHI, F. & KIRBY, T. 2012 Shock-capturing non-hydrostatic model for fully dispersive surface wave processes. *Ocean Model.* **43–44**, 23–35.

MADSEN, P. A., BINGHAM, H. B. & SCHÄFFER, H. A. 2003 Boussinesq-type formulations for fully nonlinear and extremely dispersive water waves: derivation and analysis. *Proc. R. Soc. Lond.* A **459** (2033), 1075–1104.

MADSEN, P. A., FUHRMAN, D. R. & WANG, B. 2006 A Boussinesq-type method for fully nonlinear waves interacting with a rapidly varying bathymetry. *Coast. Engng* **53**, 487–504.

MADSEN, P. A., MURRAY, R. & SØRENSEN, O. R. 1991 A new form of Boussinesq equations with improved linear dispersion characteristics. *Coast. Engng* **15**, 371–388.

MAHADEVAN, A., OLIGER, J. & STREET, R. L. 1996*a* A non-hydrostatic mesoscale ocean model, Part I: Well-posedness and scaling. *J. Phys. Oceanogr.* **269**, 1868–1880.

MAHADEVAN, A., OLIGER, J. & STREET, R. L. 1996*b* A non-hydrostatic mesoscale ocean model, Part II: Numerical implementation. *J. Phys. Oceanogr.* **269**, 1881–1900.

MARSHALL, J., HILL, C., PERELMAN, L. & ADCROFT, A. 1997 Hydrostatic, quasi-hydrostatic, and non-hydrostatic ocean modelling. *J. Geophys. Res.* **102**, 5733–5752.

NWOGU, O. 1993 Alternative form of Boussinesq equations for nearshore wave propagation. *J. Waterway Port Coast. Ocean Engng* **119**, 618–638.

OTTESEN-HANSEN, N. E. 1978 Long period waves in natural wave train. Progress Report no. 46, Institute of Hydrodynamics and Hydraulic Engineering, Technical University of Denmark, pp. 13–24.

PEREGRINE, D. H. 1967 Long waves on a beach. *J. Fluid Mech.* **27**, 815–827.

ROEBER, V. & CHEUNG, K. F. 2012 Boussinesq-type model for energetic breaking waves in fringing reef environments. *Coast. Engng* **70**, 1–20.

ROEBER, V., YAMAZAKI, Y. & CHEUNG, K. F. 2010 Resonance and impact of the 2009 Samoa tsunami around Tutuila, American Samoa. *Geophys. Res. Lett.* **37**, L21604.

SAND, S. E. & MANSARD, E. P. D. 1986 Reproducetion of higher harmonics in irregular waves. *Ocean Engng* **13**, 57–83.

SCHÄFFER, H. A., MADSEN, P. A. & DEIGAARD, R. A. 1993 A Boussinesq model for wave breaking in shallow water. *Coast. Engng* **20**, 185–202.

SHI, F., KIRBY, J. T., HARRIS, J. C., GEIMAN, J. D. & GRILLI, S. T. 2012 A high-order adaptive time stepping TVD solver for Boussinesq modelling of breaking waves and coastal inundation. *Ocean Model.* **43–44**, 36–51.

STANSBY, P. K. & ZHOU, J. G. 1998 Shallow-water flow solver with non-hydrostatic pressure: 2D vertical plane problems. *Intl J. Numer. Meth. Fluids* **28**, 541–563.

STELLING, G. S. & DUINMEIJER, S. P. A. 2003 A staggered conservative scheme for every Froude number in rapidly varied shallow water flows. *Intl J. Numer. Meth. Fluids* **43**, 1329–1354.

STELLING, G. S. & ZIJLEMA, M. 2003 An accurate and efficient finite-difference algorithm for non-hydrostatic free-surface flow with application to wave propagation. *Intl J. Numer. Meth. Fluids* **43**, 1–23.

TONELLI, M. & PETTI, M. 2012 Shock-capturing Boussinesq model for irregular wave propagation. *Coast. Engng* **61**, 8–19.

WEI, G. & KIRBY, J. T. 1995 Time-dependent numerical code for extended Boussinesq equations. *J. Waterway Port Coast. Ocean Engng* **121** (5), 251–261.

WEI, G., KIRBY, J. T. & GRILLI, S. T. 1995 A fully nonlinear Boussinesq model for surface waves. Part 1. Highly nonlinear unsteady waves. *J. Fluid Mech.* **294**, 71–92.

WU, C. H., YOUNG, C. C., CHEN, Q. & LYNETT, P. J. 2010 Efficient non-hydrostatic modelling of surface waves from deep to shallow water. *J. Waterway Port Coast. Ocean Engng* **136** (2), 104–118.

YAMAZAKI, Y. & CHEUNG, K. F. 2011 Shelf resonance and impact of near-field tsunami generated by the 2010 Chile earthquake. *Geophys. Res. Lett.* **38**, L12605.

YAMAZAKI, Y., CHEUNG, K. F. & KOWALIK, Z. 2011*a* Depth-integrated, non-hydrostatic model with grid nesting for tsunami generation, propagation and runup. *Intl J. Numer. Meth. Fluids* **67**, 2081–2107.

YAMAZAKI, Y., KOWALIK, Z. & CHEUNG, K. F. 2009 Depth-integrated, non-hydrostatic model for wave breaking and runup. *Intl J. Numer. Meth. Fluids* **61**, 473–497.

YAMAZAKI, Y., LAY, T., CHEUNG, K. F., YUE, H. & KANAMORI, H. 2011*b* Modelling near-field tsunami observations to improve finite-fault slip models for the 11 March 2011 Tohoku earthquake. *Geophys. Res. Lett.* **38**, L00G15.

YUAN, H. & WU, C. H. 2004 A two-dimensional vertical non-hydrostatic sigma model with an implicit method for free-surface flows. *Intl J. Numer. Meth. Fluids* **44**, 811–835.

ZELT, J. A. 1991 The runup of non-breaking and breaking solitary waves. *Coast. Engng* **15**, 205–246.

ZHOU, J. G. & STANSBY, P. K. 1999 An arbitary Lagrangian–Eulerian σ (ALES) model with non-hydrostatic pressure for shallow water flows. *Comput. Meth. Appl. Mech. Engng* **178**, 199–214.

ZIJLEMA, M. & STELLING, G. S. 2005 Further experiences with computing non-hydrostatic free-surface flows involving water waves. *Intl J. Numer. Meth. Fluids* **48**, 169–197.

ZIJLEMA, M. & STELLING, G. S. 2008 Efficient computation of surf zone waves using the nonlinear shallow water equations with non-hydrostatic pressure. *Intl J. Numer. Meth. Fluids* **55**, 780–790.

ZIJLEMA, M., STELLING, G. S. & SMIT, P. 2011 SWASH: an operational public domain code for simulating wave fields and rapidly varied flows in coastal waters. *Coast. Engng* **58**, 992–1012.